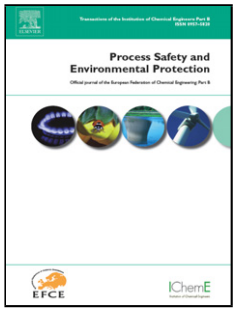


Title: Removal of fluoride from aqueous solution by adsorption on NaP:HAp Nanocomposite using response surface methodology

Authors: M. Zendehdel, B. Shoshtari-Yeganeh, H. Khanmohamadi, G. Cruciani

PII: S0957-5820(17)30094-0
DOI: http://dx.doi.org/doi:10.1016/j.psep.2017.03.028
Reference: PSEP 1019

To appear in: *Process Safety and Environment Protection*

Received date: 22-11-2016
Revised date: 18-3-2017
Accepted date: 22-3-2017

Please cite this article as: Zendehdel, M., Shoshtari-Yeganeh, B., Khanmohamadi, H., Cruciani, G., Removal of fluoride from aqueous solution by adsorption on NaP:HAp Nanocomposite using response surface methodology.Process Safety and Environment Protection http://dx.doi.org/10.1016/j.psep.2017.03.028

# Removal of fluoride from aqueous solution by adsorption on NaP:HAp Nanocomposite using response surface methodology

**M. Zendehdel[a*], B. Shoshtari-Yeganeh [a], H. Khanmohamadi [a], G. Cruciani[b]**

[a] Department of Chemistry, Faculty of Science, Arak University, Arak38156-8- 8349; Iran

[b] Department of Physics and Earth Sciences, University of Ferrara , Via G. Saragat 1, I-44122 Ferrara, Italy

**E-mail: m-zendehdel@araku.ac.ir**

## Highlights

- Synthesized simple and friendly environmentally adsorbent via hydrothermal process.
- Final concentration of residual fluoride ion was determined by new receptor.
- RSM was used for investigation of optimized effective parameters on fluoride removal.
- The adsorption process followed a pseudo-second order rate law.

## Abstract

The new nanocomposite of NaP-Hydroxyapatite (NaP:HAp) has been developed for removal of fluoride from aqueous solution. NaP: HAp nanocomposite has been characterized by using different method such as: X-ray diffraction (XRD), Fourier transform infrared spectroscopy (FT-IR), scanning electron microscope (SEM), Energy Dispersive X-ray analysis (EDAX), surface area (BET) and thermal gravimetric analysis (TGA). Box–Behnken design with three-level and four-factor has been employed for determination of effective process parameters such as solution pH (4-11), temperature (25-55˚C), initial adsorbent dose (1-3 g) and initial fluoride concentration (5-25 mg/L) on removal of fluoride from aqueous solution. After 29 batch runs, Quadratic model was established by regression analysis of the experimental data obtained from 29 batch runs. Quantity uptake of fluoride was evaluated using the Langmuir, Freundlich and Dubinin–Radushkevich (DR) models. The rate of adsorption was rapid and followed pseudo-second-order kinetics for this adsorbent. Moreover, thermodynamic parameters ($\Delta H^{\circ}$, $\Delta G^{\circ}$, $\Delta S^{\circ}$) for fluoride sorption on NaP:HAp nanocomposite was also studied from the temperature dependence. The significant novelty of this work is

the simple preparation of a new nanocomposite from hydroxyapatite and zeolite that increased stability of HAp in different pH and temperature. Also, this nanocomposite shows high capacity for adsorption of fluoride related of other sorbent and reusable for several times that makes this method nearly green and friendly environmentally.

Keyword: NaP:Hydroxyapatite, Fluoride removal, Box-Behnken design, Response surface technique, Thermodynamic parameters, kinetic, Isotherm prameters

**1. Introduction**

Water is most abundant and is an essential component of our life supporting system. The removal of toxic ions and recovery of valuable ions from mine wastewaters, soils and waters have been important in economic and environmental problems. Some of these hazard materials such as fluoride ions are accumulated in living organisms and produce diseases and disorders. Fluoride bearing rocks such as fluorapatite, fluorspar, cryolite, and hydroxylapatite are the main sources of fluoride in ground water. Many factors such as pH, temperature, concentration of calcium and bicarbonate ions and solubility of fluoride minerals in water have an impact on the amount of fluoride content in the ground water [1]. Removal of fluoride from water is very important because high levels of fluoride can cause drastic problems for humans such as bone fluorosis, dental caries and lesions of the thyroid, endocrine glands, and brain [2], Therefore, management of fluoride is necessary for public health. In fact, Low level of fluoride is useful for human, however, the beneficial fluoride concentration range for human health is very small. According to the World Health Organization guidelines (WHO), the maximum limit of fluoride concentration in drinking water is $1.5 mgL^{-1}$ [3]. Nevertheless, high level of fluoride in aqueous solution is a world-wide problem including various regions in North Africa, China, Mexico and Asia [2]. So far, various methods have been applied for the defluoridation from aqueous environments, such as ion-exchange, adsorption, precipitation, electrodialysis and electrochemical methods [4]. Among these methods, Adsorption has been found as the most effective used method for removal of fluoride based on low maintenance cost, flexible process and simplicity of design [5]. In recent years, different low-cost adsorbent such as synthetic resin [6], activated alumina [7], carbon nano tubes [8], bone char [9], fly ash [10] and other materials have been used for removal of fluoride ion [11]. Notwithstanding, fluoride adsorption capacity of the most conventional adsorbent is not enough for wide applications so in recent years, many efforts have been carried out to develop new and effective materials for removal of fluoride. For instance, in many literatures, using of adsorbent

with micron-sized particles for removal of fluoride was reported, But in recent years, nano materials with high surface to volume ratio and short diffusion route have been used as an effective sorbent of fluoride from aqueous solution [12]. Hydroxyapatite (HAp, $Ca_{10}$ $(PO_4)_6(OH)_2$) is the main mineral essential of vertebrate skeletal systems. It is the well-known component with high application as an adsorbent in purification of wastewater [13] and it has been used in biomedicine, biosensor, catalyst or catalyst support and used as a bone substitute and ceramic implants [13]. Although, Hydroxyapatite has been studied as fluoride sorbent in different conditions but various limitations such as: low mechanical reliability in wet environment, thermal and absorption in narrow range of pH [14]. Thus, one of the important goals for developing synthesize method is focusing on size and hybrid material factors of HAp.

Zeolites are naturally aluminosilicates which can be also obtained by synthesis and characterized by high internal and external surface areas. Several types of moieties like water and alkaline/alkaline earth metals can be hosted porous and channels of zeolite which literature review shows these cations have good efficiency to fluoride adsorption as well [15]. NaP zeolite with a gismondine (GIS) framework topology and interesting channels of 0.31 nm × 0.44 nm in [100] and 0.26 nm × 0.44 nm in [010] [16] has a good potential for adsorption of small gases, liquid molecules, and hazard materials [17]. According to above introduction, zeolite: HAp nanocomposite may be a potential adsorbent for simultaneous removal of fluoride from aqueous solution because of zeolite: HAp may have characteristics of both HAp and zeolite jointly.

Response surface methodology (RSM) is a collection of mathematical and statistical techniques for empirical model building and also can avoid the limitations of conventional methods. Design of experiments (DOE) and response surface methodology (RSM) is very useful for modeling mechanism parameters, specifically in adsorption or removal process [18]. Mainly RSM is used to determine the most favorable operational conditions for a particular system or to check a region that satisfies the operational specifications [19]. The present study focused on the synthesis of NaP: Hydroxyapatite nanocomposite which is able effectively to remove fluoride from aqueous solution. We successfully synthesized this adsorbent and characterized by XRD, FT-IR, SEM, EDAX, BET and TGA studies. Also, effect of various factors include initial concentration, initial pH solution, adsorbent dosage and temperature on fluoride removal from aqueous solution by NaP:HAp nanocomposite were investigated by using Box-Behnken Design (BBD) in Response Surface Methodology (RSM). A new azo-azomethine colorimetric receptor and UV-vis spectrophotometer were used to determine the final concentration of residual fluoride ion in solution. Different models of isotherm

adsorbent such as (Freundlich, Langmuir, Temkin, and Dubinin-Radushkevich) were used to discuss the mechanism of removal by this adsorbent. Kinetic models and thermodynamic parameters also described in this study.

.

## 2. Experimental

### 2.1. Material and instrument

The powder of Hydroxyapatite was prepared by using calcium nitrate (CNT), potassium dihydrogen phosphate (KPP), ammonia and deionized water. Silica gel, sodium hydroxide and aluminum hydroxide were used for preparation of zeolite, sodium hydroxide and Hydrochloric acid (HCl) for adsorption/desorption experiment (all chemical materials supplied by Merck). The preliminary XRD identification of crystalline phases was carried out by a Philips X'Pert diffractmeter operating with Cu-Kα radiation. FT-IR of the samples was characterized by Unicom Galaxy Series FT-IR 5000 in region of 200-4000 $cm^{-1}$. Electronic spectrum measurements were carried out using an optizen 3220 UV spectrophotometer in the range of 200-900 nm.

### 2.2. Synthesis and characterization of Hydroxyapatite

Briefly, precursor solutions (1M CNT, 0.6M KPP) were prepared by dissolution of pure soluble salts (calcium nitrate and potassium dihydrogen phosphate) under continuously stirring at ambient temperature conditions. Then, solution of CNT was added slowly to the KPP solution. In addition, pH of the solution was adjusted to 11 by mixing it with ammonia (17% W/V) and reaction mixture was stirred for 1 h then kept 24 h in an ambient temperature in order to complete reaction. Furthermore, resulting suspension was filtrated and washed with hot distilled water for removal of ammonium, potassium and nitrate ions. Subsequently, powder sample was heated in an oven for 24h in the temperature of 40˚C and the obtained white powder was calcined for 1h at 600˚C. The process was accomplished by evaluation of the resulting powder using Fourier transform infrared spectroscopy (Galaxy series FT-IR 5000 spectrometer) and examining powder morphology by with a scanning electron microscopy test (Philips XL30 electron microscope).

### 2.3. Synthesis and characterization of NaP:HAp nanocomposite

Zeolite of NaP was selected as a second material and for this purpose of aged zeolite gel preparation, 16.13 g of sodium silicate (containing 19.8 wt% $SiO_2$), 6 ml of initiator (with the molar composition $16Na_2O$: $Al_2O_3$: $15SiO_2$: $320H_2O$ and aged at 320˚C for 32h), 13.2 ml of sodium hydroxyl (24wt %) and 5.2 g of deionized water were used. For the preparation of NaP:HAp nanocomposite different amounts of HAp were added to zeolite gel and mixture was stirred for 15 min continuously. In order to prepare of nanocomposite, the mixture was then placed in an autoclave at

100˚C for 26 h. Next, the precipitated sample filtrated and washed with deionized water repeatedly until to reach pH of 7. The resulting product was then dried at room temperature for 24h. Also, the obtained powder was evaluated by Fourier transform infrared spectroscopy (Galaxy series FT-IR 5000 spectrometer) and analyzed by standard X-ray diffraction using a Philips X'Pert diffractometer operating with Cu-Kα radiation. The angle was scanned from 5° to 95° at a scanning step 0.02°. Additionally, powder was also used for scanning electron microscopy, Energy Dispersive X-ray analysis, surface area and thermal gravimetric analysis. Moreover, the results of analysis were explored in result section and the obtained powders were used as an adsorbent for removal of fluoride ions form aqueous solution using batch experiment method.

**2.4. Experimental procedure**

Batch experiment was used to investigate the adsorption of fluoride ion on NaP:HAp nanocomposite. Different concentrations of fluoride solutions that were in the range of 5-25 mg/L were prepared by stock solution with 1000 mg/L. Then, adsorbent dosage in the range of 1-3 g/L added to 25 mL of each solution. pH adjustments made in the range of 4-11 and then, suspension was stirred at different temperature (25-55 ˚C) for 60 minutes. The solution was filtrated and residual fluoride ion was analyzed. Sorption isotherm studies was conducted by adding 3 g/L of sorbent to a 25 mL of solution containing various concentration of fluoride ion ( 5, 10, 15, 20, 25 mg/L) with pH value of 6. After 1h, the suspension was filtrated and eventually residual solution was analyzed.

A new azo-azomethine colorimetric receptor and UV-vis spectrophotometer were used to determine the final concentration of residual fluoride ion in solution that tailoring in our laboratory for the first time. Upon the addition of residual solution to receptor, it was showed remarkable color change from light yellow to orange. Detect of $F^-$ was measured with a UV-vis spectrophotometer at a wavelength of 490 nm [20].

Amount of fluoride adsorbed (mg/g) onto the NaP:HAp nanocomposite was calculated according to the following equation:

$$q_e = \frac{(C_\circ - Ce)V}{W} \qquad (1)$$

Where, $C_0$ is the initial fluoride concentration (mg/L) and $C_e$ is the equilibrium concentration (mg/L) respectively. $q_e$ (mg/g) is the amount of adsorbate adsorbed per unit mass of adsorbent, V is the volume solution (in liter) and W is the weight of NaP:HAp nanocomposite (in grams).

The removal efficiency of fluoride ions from aqueous solution (in percent) was calculated by the following equation as well:

$$\%\text{Removal} = \frac{C_\circ - Ce}{C_\circ} \times 100 \qquad (2)$$

**2.5. Box-Behnken experimental design**

The four factors Box-Behnken design with three levels experimental data was established using Design expert software (10.0.1 trial version). The factor levels were being coded as -1, 0 and 1 for low, middle and high values respectively [21, 22]. The range and levels used in the experiments are listed in Table 1. in order to determination of the optimized process parameters a total of 29 runs were done as well as the experiments which were carried out according to the actual experimental design matrix (results shown in Table 2). A second-order polynomial model has been developed to identify all possible interactions of input factors obtained from the Box–Behnken model:

$$Y = \beta_\circ + \Sigma\beta_i X_i + \Sigma\beta_{ii} X_{ii}^2 + \Sigma\beta_{ij} X_i Xj + \varepsilon \qquad (3)$$

Where Y is the percentage of fluoride adsorbed, $\beta_\circ$ is the constant coefficient, $\beta_i$, $\beta_{ii}$ and $\beta_{ij}$ are the linear coefficient, quadratic coefficient and different interaction between input factors of $X_i$ and $X_j$ respectively and $\varepsilon$ is the error of model [23].

| Factors range and levels (coded) | -1 | 0 | +1 |
|---|---|---|---|
| Initial concentration (mg/L) | 5 | 15 | 25 |
| Initial pH | 4 | 7.5 | 11 |
| Adsorbent dosage (g/L) | 1 | 2 | 3 |
| Temperature (˚C) | 25 | 40 | 55 |

Table.1. Factors and levels used in the factorial design.

| Coded values of the variables | | | | | |
|---|---|---|---|---|---|
| Experimental run | Concentration(A) | pH(B) | Adsorbent dosage(C) | Temperature (˚C) | %R |
| 1 | -1 | -1 | 0 | 0 | 50 |
| 2 | 1 | 0 | 0 | 1 | 62.7 |
| 3 | 0 | 0 | 0 | 0 | 50.8 |
| 4 | 0 | -1 | 0 | -1 | 49.12 |
| 5 | 0 | 1 | 1 | 0 | 37.06 |
| 6 | -1 | 0 | 0 | 1 | 96.3 |
| 7 | -1 | 0 | -1 | 0 | 55.5 |
| 8 | 1 | 0 | -1 | 0 | 22.65 |
| 9 | 0 | 1 | 0 | 1 | 37 |
| 10 | 0 | -1 | 0 | 1 | 55 |
| 11 | -1 | 0 | 0 | -1 | 80 |
| 12 | 0 | 1 | -1 | 0 | 10.5 |
| 13 | 0 | 0 | 1 | -1 | 58.5 |
| 14 | -1 | 0 | 1 | 0 | 85.43 |
| 15 | 0 | 0 | -1 | 1 | 12.7 |
| 16 | -1 | 1 | 0 | 0 | 76 |
| 17 | 0 | 0 | -1 | -1 | 12.6 |
| 18 | 0 | 0 | 0 | 0 | 65.27 |
| 19 | 0 | 0 | 1 | 1 | 66.8 |
| 20 | 0 | 0 | 0 | 0 | 49.86 |
| 21 | 1 | 0 | 1 | 0 | 57.4 |
| 22 | 0 | -1 | -1 | 0 | 12.4 |
| 23 | 1 | 1 | 0 | 0 | 31.5 |
| 24 | 0 | 1 | 0 | -1 | 35.33 |
| 25 | 0 | 0 | 0 | 0 | 51.33 |

| | | | | | |
|---|---|---|---|---|---|
| 26 | 0 | 0 | 0 | 0 | 49.8 |
| 27 | 1 | 0 | 0 | -1 | 56.9 |
| 28 | 0 | -1 | 1 | 0 | 62.09 |
| 29 | 1 | -1 | 0 | 0 | 48.35 |

Table.2. Box-Behnken design matrix for four variables together with the observed response.

**3. Results and discussion**

**3.1. Characterization of NaP:HAp nanocomposite**

**3.1.1. Powder X-ray diffraction studies**

Fig 1a-d shows the XRD pattern of NaP:HAp nanocomposite with different ratio (NaP:HAp ratio: 1:1,1:2,1:4,1:6) and Fig.2 shows HAp alone which was collected and fitted by the Rietveld method. X-ray diffraction analysis shows the presence of gismondine-like zeolite in the synthesized sample for 1:1 ratio (Fig 1a) with reflections on 2θ = 12.48˚, 17.92˚, 21.79˚, 28.1˚and 33.4˚ [24]. Also, analyzing the other peaks observed by XRD pattern of synthesized nanocomposite of NaP:HAp. The minor and broad peak at about 2θ = 29˚ corresponding to Hydroxyapatite. This suggests that the zeolite pores could also be incorporated by nano particles of HAp due to very small nano size that in agreement to what reported by other researchers [25-27]. In addition, the obtained broad diffraction peak around 29° 2θ is basically, due to the presence of nano-hydroxyapatite (crystallite size ~ 8 nm) which confirmed by rietveld fit that also is based on the hydroxyapatite crystal structure model of El Feki et al. [28] in the P63/m space group with refined unit cell parameters: a = 10.53(1) Å, c = 6.88(1) Å. Additionally, results show that with increasing the percent of hydroxyapatite the reflections of NaP and HAp phases can be observed as well, which demonstrate both hydroxyapatite and NaP phases present as a hybrid form.

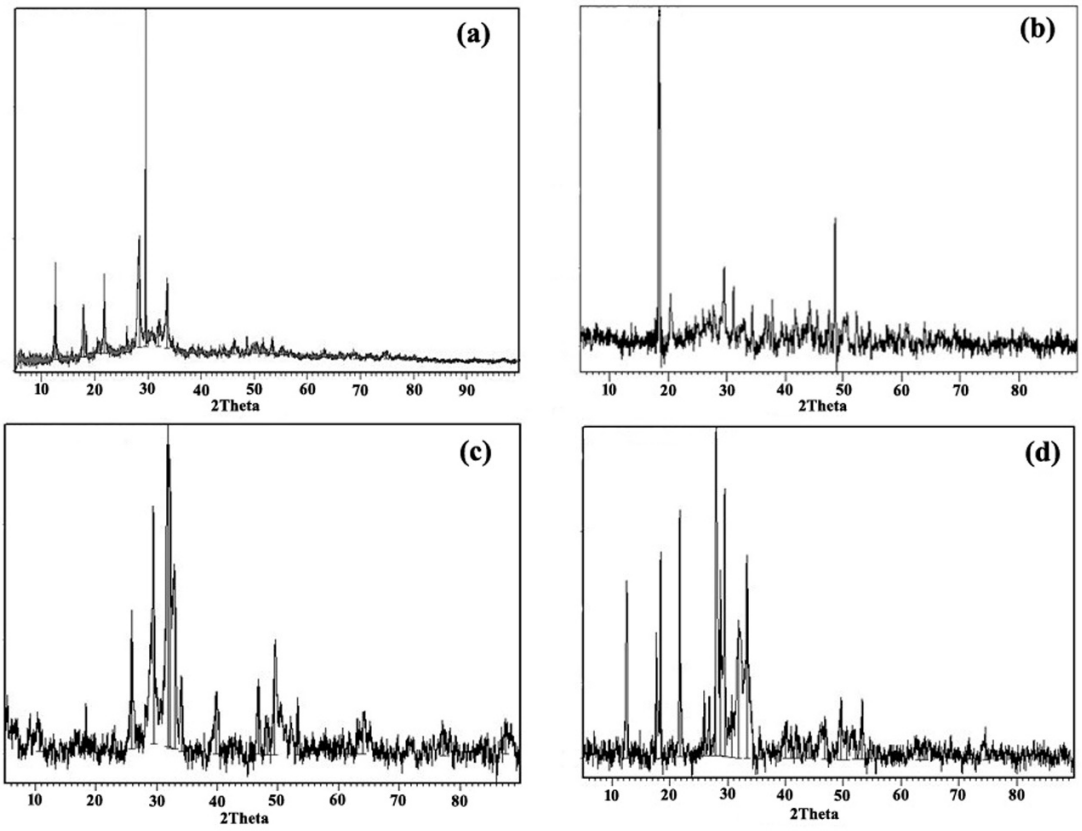


Fig.1. a-d) XRD pattern of NaP:HAp nanocomposite with different ratio (NaP:HAp ratio: 1:1,1:2,1:4,1:6)

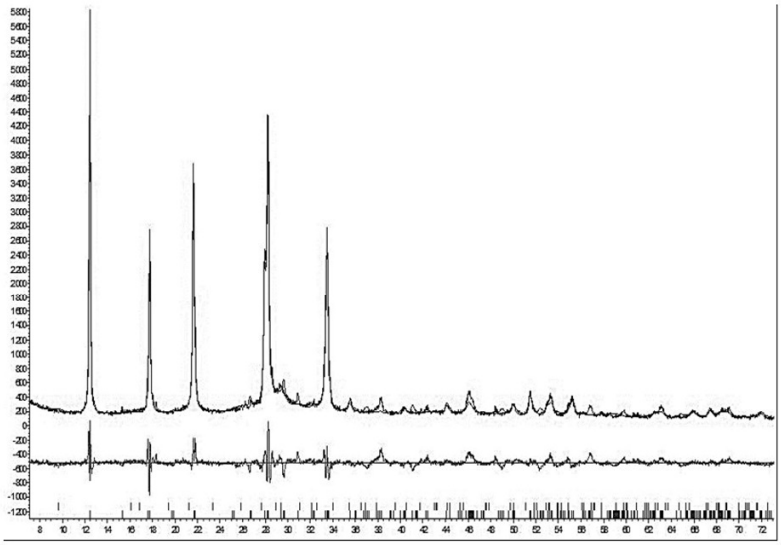


Fig.2. Rietveld fit of XRD pattern of NaP:HAp nanocomposite with ratio of 1:1

**3.1.2. FT-IR analysis**

The FT-IR spectra in Fig 3a-e showed the characteristic adsorption bands of a NaP (a), HAp (b) and nanocomposite with different ratio ( NaP:HAp ratio : 1:1 (c), 1:2 (d), 1:4 (e) and 1:6 (f)). In Fig 3a, the band at 1012 $cm^{-1}$ corresponded to internal tetrahedral asymmetrical stretching and the band at 799 $cm^{-1}$ and 437 $cm^{-1}$ is corresponding to amorphous $SiO_2$ stretching vibration and $TO_4$ (T=Si, Al) bending mode respectively [29]. The two bands at 3466 and 1653 $cm^{-1}$ are assigned to the hydroxyl group stretching vibration and H-O-H bending vibration respectively [30]. In Fig 3b, band centered at 3574 $cm^{-1}$ is assigned to the stretching vibration of OH in hydroxyapatite lattice. Also, two bands at 1456$cm^{-1}$ and 854 $cm^{-1}$ are assigned to carbonate group and the band at 1035 $cm^{-1}$ and the band at 962 $cm^{-1}$ are attributed to P=O stretching vibration of $PO_4^{3-}$ and symmetric P=O stretching vibration ($\nu_1$). Plus, the band at 474 $cm^{-1}$ and the two bands at 567 and 601 $cm^{-1}$ are assigned to the $\nu_2$ and $\nu_4$ bending vibration of phosphate group [31].

In Fig 3c, the two bands at 3533 and 1653 $cm^{-1}$ corresponded to the OH stretching and bending vibration respectively. Two bands at 1028 and 605 $cm^{-1}$ corresponded to the P=O stretching vibration of $PO_4^{3-}$ and bending vibration of phosphate group respectively. Also, the band at 742 $cm^{-1}$ is assigned to amorphous $SiO_2$ stretching vibration and the band at 435 $cm^{-1}$ is attributed to the $TO_4$ (T=Si or Al) bending mode [29]. For more study, we characterized another ratio of NaP:HAp nanocomposite (ratio: 1/2, 1/4, 1/6). As shown Fig 3d-f, the result shows that with increasing the

percent of hydroxyapatite, the intensity of relation peaks increased. Showing the characteristic band of Hydroxyapatite and NaP zeolite in Fig 3c, also confirms the presence of two phases in nanocomposite.

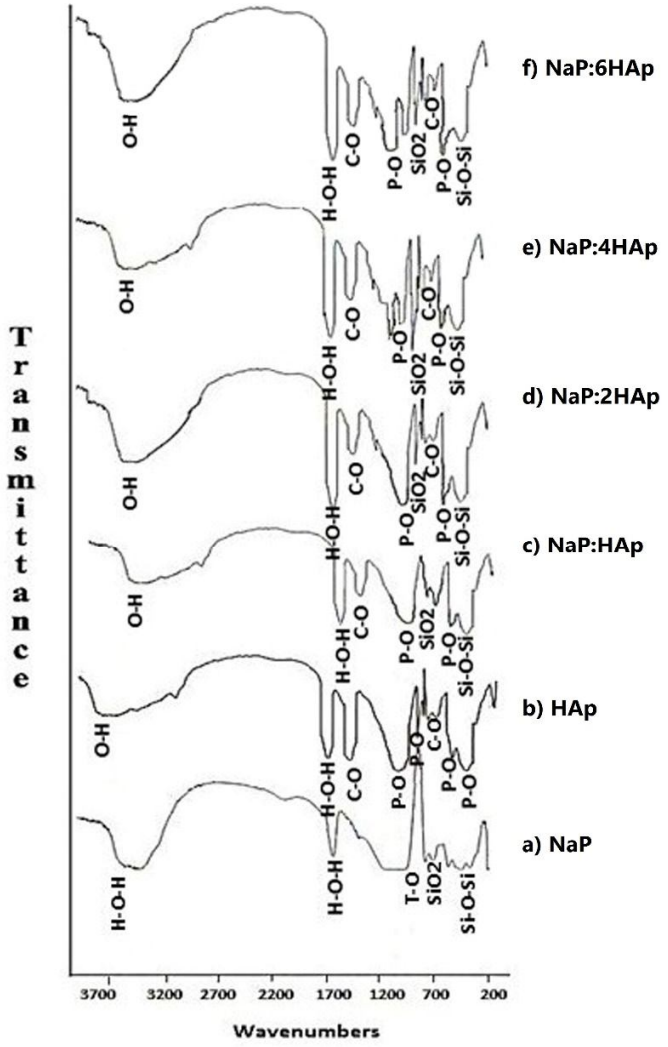


Fig.3. FT-IR spectra of NaP (a), HAp (b) and NaP:HAp with different ratio(1:1 (c), 1:2 (d), 1:4 (e) and 1:6 (f)

### 3.1.3. SEM and EDX studies

NaP:HAp nanocomposite with different ratio and Hydroxyapatite nanoparticles were examined by SEM. Fig 4a-f is SEM micrograph for NaP:HAp nanocomposite and Hydroxyapatite respectively. Similar to other observations found

in the literature, both cactus-like and diamond like morphology with the 1-2 μm size of each diamond-shape particle were appeared in the SEM image of NaP:HAp nanocomposite [32]. Also, we can see with increasing the percent of HAp diamond like morphology for NaP zeolite has become visible. From a Hydroxyapatite image (Fig 4e, f), the result illustrates that the synthesized Hydroxyapatite powder were particle shaped with the diameter of 40-70 nm and were made. Moreover, the presence of much smaller nano size of Hydroxyapatite particles in NaP:HAp nanocomposite can be explained by the dispersing agent of zeolite network for the Hydroxyapatite nanocrystal. In fact, it can be considered that the zeolite acted as a dispersing agent and distributed nano crystal of Hydroxyapatite over the external surface of zeolite and/or incorporation of NaP pores which can be observed the direct relation of the increasing HAp particle with increasing the percent of it.

Atomic percent of Ca, P, Na, Al, Si and O were presented in Table 3 from EDX analyzing of HAp and NaP:HAp, NaP: 4HAp and NaP:6HAp nanocomposite. According to the results reported in Table 3, we can see hydroxyapatite sample and different ratio of NaP:HAp nanocomposite contained atomic Ca/P ratio of 1.53 to 1.61 which is close to the stoichiometric hydroxyapatite. Also, presence of Na, Al and Si elements that attributed to the NaP zeolite in these nanocomposites and minor presence of Ca and P elements in NaP:HAp can be related to the low density of hydroxyapatite loaded onto the NaP zeolite or encapsulation in to the zeolite pores [25, 26].

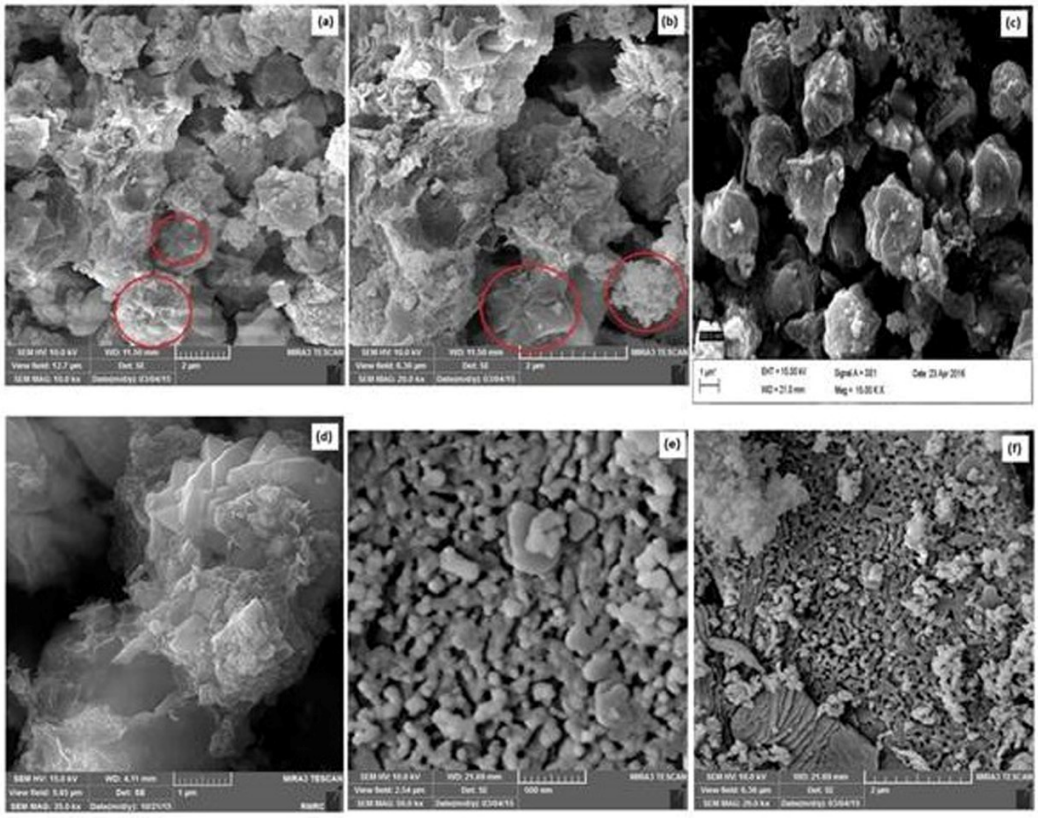

Fig.4. SEM micrograph of (a-b) NaP:HAp nano composite with ratio of 1:1, (c) NaP:4HAp, (d) NaP:6HAp and (e,f) HAp

| sample | ca | P | Na | Al | Si | O | Ca/P |
|---|---|---|---|---|---|---|---|
| HAp | 14.6 | 9.42 | - | - | - | 70.87 | 1.55 |
| NaP:HAp | 8.56 | 5.57 | 4.45 | 6.78 | 13.04 | 55.30 | 1.53 |
| NaP:4HAp | 13.55 | 8.39 | 4.43 | 6.38 | 14.68 | 53.74 | 1.61 |
| NaP:6HAp | 15.84 | 9.96 | 2.14 | 5.28 | 14.96 | 50.8 | 1.59 |

Table.3. Atomic percent of elements and Ca/P ratios obtained by EDX.

**3.1.4. BET analysis**

The specific surface areas and pore volume of the adsorbent were estimated by nitrogen adsorption at relative pressures ($P/P_0$) in the range of 0.008–0.5. The BET data for the NaP zeolite after loading of hydroxyapatite shows a small decrease from 45 $m^2/g$ to 35.62 $m^2/g$ and 30.23 for NaP:HAp ratio 1:1 and 1:4, respectively. Also, the total pore volume of NaP zeolite 0.151 change to 0.141 and 0.135 $cm^3/g$ for NaP:HAp ratio 1:1 and 1:4, respectively. Since the zeolite framework structure is not affected by incorporated HAp as shown by the XRD pattern and SEM earlier, the

reduction of surface area and pore volume outcomes, might be due to the presence of small amount of HAp in the cavities of zeolite [33].

The $N_2$ adsorption/desorption isotherms of NaP:HAp with 1:1 and 1:4 ratios are given in Fig 5a-b. These isotherms can be classified as type I characteristic of the microporous materials [34].

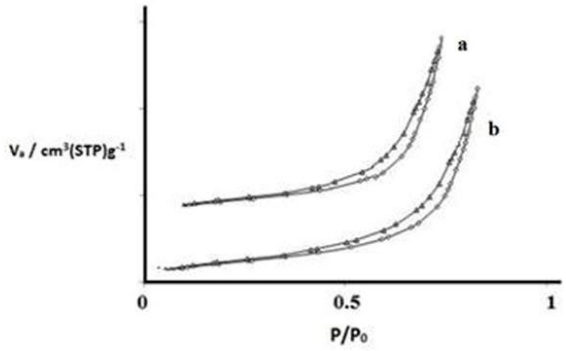


Fig.5. The $N_2$ adsorption/desorption isotherms of NaP:HAp with 1:1 ratio (a), 1:4 ratio (b)

**3.1.5. Thermogravimetric analysis (TGA)**

Table 4 demonstrates the weight loss for NaP and NaP:HAp nanocomposite with different percent of HAp. According to the TG-DSC curves of the NaP zeolite by Z. Huo et al [32], it exhibits two mass loss steps for NaP zeolite. In general, first step with weight loss about 10% event in the temperature range 25–200˚C can be attributed to an endothermic DTA peak and ascribed to release of water while the second event with loss of about 4% in the temperature range 200–400˚C can be attributed to removal of hydroxyl groups. A third event marked by weak endothermic peaks in the temperature range 400–800˚C which is not connected with weight losses and might be related to some phase transformations known to occur in gismondine-like structures [35, 36].

Likewise, the weight loss of NaP:HAp nanocomposite with different ratio exhibits three mass loss steps according to the TG curve. The first event in the temperature range 30-200˚C was ascribed to losses of adsorbed water in NaP zeolite and HAp. Removal of the hydroxyl group of zeolite and condensation of hydrogen phosphate groups to form pyrophosphates ($P_2O_7^{2-}$) in the hydroxyapatite can be event in the temperature range 200-500˚C and the corresponding weight loss in the last step in the temperature at about 800˚C was attributed to the phase transformation of zeolite and the conversion of $P_2O_4^{4-}$ to form $PO_4^{3-}$[37, 38]. The results show that with increasing the percent of hydroxyapatite, the weight loss is increased at second and third steps.

| **Temperature range(˚C)** | **Weight loss(%) NaP** | **Weight loss(%) NaP:HAp** | **Weight loss(%) NaP:2HAp** | **Weight loss(%) NaP:4HAp** | **Weight loss(%) NaP:6HAp** |
|---|---|---|---|---|---|
| **30-200** | **10.00** | **11.85** | **12.11** | **12.01** | **10.08** |
| **200-500** | **4.10** | **5.06** | **7.95** | **9.99** | **14.96** |
| **500-800** | **4.2** | **4.65** | **5.97** | **10.97** | **17.73** |

Table.4. The loss percent of NaP and NaP:HAp nanocomposite with different percent.

### 3.2. Box-Behnken statistical analysis

Initial concentration, initial pH, adsorbent dosage and temperature are the most important parameters which affect the efficiency of fluoride ion by NaP:HAp nanocomposite. The Box–Behnken design was used for exploring different combined parameters and for evaluating the combined effects of those factors. In the present work, linear, two factor interaction (2FI), quadratic and cubic models were used to analysis experimental data in order to obtain the regression equations. To determine the adequacy of models to represent fluoride by NaP:HAp nanocomposite, two different tests namely the sequential model sum of squares and the model summary statistics, were conducted and the results are tabulated in Table 5.

| Source | std. Dev | R-Squared | Adjusted R-Squared | Predicted R-Squared | PRESS | |
|---|---|---|---|---|---|---|
| Linear | 15.94 | 0.5492 | 0.4741 | 0.3027 | 9434.94 | |
| 2FI | 17.39 | 0.5974 | 0.3738 | -0.2951 | 17522.58 | |
| Quadratic | 8.06 | 0.9327 | 0.8655 | 0.6676 | 4496.61 | suggested |
| Cubic | 8.46 | 0.9683 | 0.8519 | -1.7029 | 36569.56 | aliased |

Table.5. Adequacy of the model tested.

In fact, cubic model was found to be aliased and the results from the sequential model indicated that the p value was lower than 0.01 from quadratic model. From model summery statistic, it can be seen that the quadratic model has

maximum ″Adjusted R-Squared″ and ″Predicted R-Squared″ values. Consequently, the quadratic model could be used for further analysis as well. For this study, the fluoride uptake by NaP:HAp nanocomposite could be described as:

$$Y(\%) = 53.41 - 13.73\times A - 4.13\times B + 20.08\times C + 3.25\times D - 10.71\times AB + 1.20\times AC - 2.87\times AD - 5.78\times BC - 1.05\times BD + 2.05\times CD + 14.89\times A^2 - 12.53\times B^2 - 13.87\times C^2 + 2.42\times D^2 \quad (4)$$

ANOVA is a statistical technique that subdivides the total variation in a set of data into component parts associated with specific sources of variation for the purpose of testing hypotheses on the parameters of the model [39]. The results from ANOVA for the quadratic equation were given in Table 6 and indicates that the model F-value of 10.33 admits the point that the model was significant. Furthermore, as shown in Table 6, the chance of $p < 0.0001$ also suggests that the model was significant. In Table 5, predicted $R^2$ and Adjusted $R^2$ are 0.6765 and 0.8663 respectively, so it was clearly shown that only approximately 2% of the total variation could not be explained by the model. In this manner, A and C were highly significant factors and B, $A^2$, $B^2$, $C^2$ and AB were significant factors and other factors that the value of P were greater than 0.1000 were not significant. Data were also analyzed to check the normality of the residuals, as shown in Fig 6. It can be seen from Fig 6 that the data on this plot were reasonably close to a straight line ($R^2$= 0.9331). The correlation between actual and predicted values of (%Y) for the adsorption of fluoride on NaP:HAp nanocomposite was shown in Fig 7. Hence, the results suggest that the developed model was adequate in predicting the response variables for the experimental because residual results were distributed near the diagonal line.

| source | Sum of squares | df | Mean square | F-value | P-value Prob>F |
|---|---|---|---|---|---|
| Model | 12619.78 | 14 | 901.41 | 13.87 | <0.0001 |
| A-concent | 2261.33 | 1 | 2261.33 | 34.79 | <0.0001 |
| B-pH | 204.77 | 1 | 204.77 | 3.15 | 0.0976 |
| C-adsorbent | 4837.27 | 1 | 4837.27 | 74.42 | <0.0001 |
| D-temp | 127.08 | 1 | 127.08 | 1.96 | 0.1838 |
| AB | 459.03 | 1 | 459.03 | 7.06 | 0.0188 |
| AC | 5.81 | 1 | 5.81 | 0.089 | 0.7694 |
| AD | 33.06 | 1 | 33.06 | 0.51 | 0.4874 |

| | | | | | |
|---|---|---|---|---|---|
| BC | 133.75 | 1 | 133.75 | 2.06 | 0.1734 |
| BD | 4.43 | 1 | 4.43 | 0.068 | 0.7978 |
| CD | 16.81 | 1 | 16.81 | 0.26 | 0.6190 |
| $A^2$ | 1438.58 | 1 | 1438.58 | 22.13 | 0.0003 |
| $B^2$ | 1018.41 | 1 | 1018.41 | 15.67 | 0.0014 |
| $C^2$ | 1247.88 | 1 | 1247.88 | 19.20 | 0.0006 |
| $D^2$ | 37.98 | 1 | 37.98 | 0.58 | 0.4573 |
| Residual | 909.96 | 14 | 65.00 | | |
| Lack of Fit | 732.53 | 10 | 73.25 | 1.65 | |
| Pure Error | 177.43 | 4 | 44.36 | | |
| Cor Total | 13529.74 | 28 | | | |

Table.6. ANOVA for response surface reduced quadratic model.

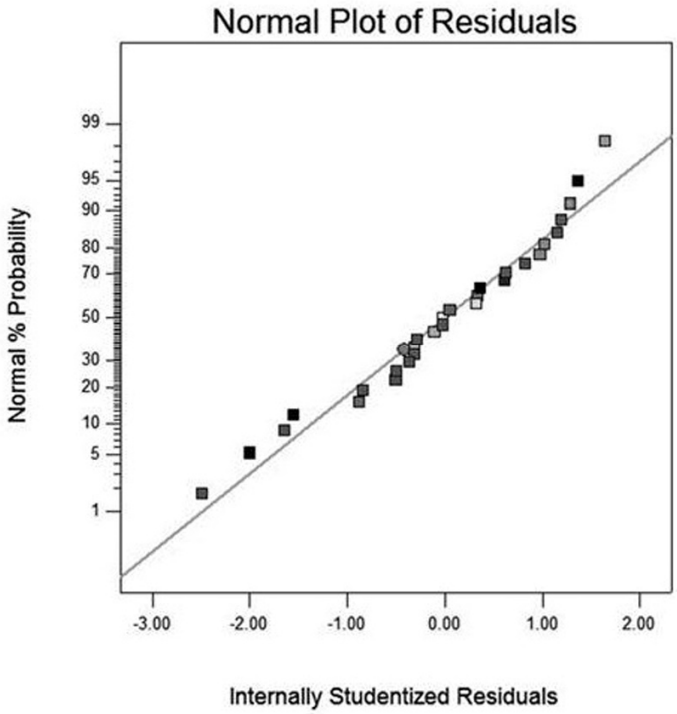


Fig.6. Normal% probability versus residual error

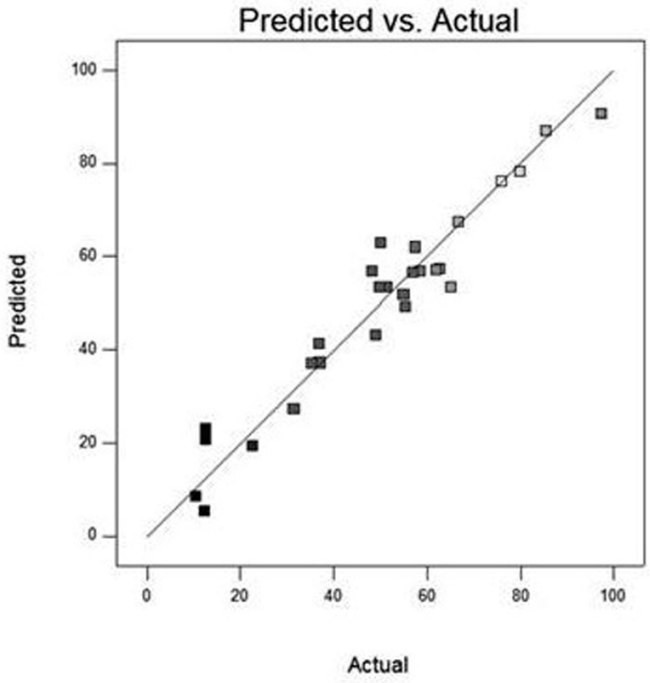


Fig.7. Predicted response versus actual response

**3.3. Effect of various parameters on fluoride removal efficiency**

**3.3.1. Effect of HAp dosage add**

For investigating of HAp dosage effect in NaP:HAp nanocomposite, batch mode experiments were performed and the results are shown by Fig 8. All the experiments with different ratio of HAp were carried out at ambient temperature. All adsorbents (3g/L) added to 25 mL of 5mg/L fluoride solution with pH 7 and stirred for 1h. It was observed that the ratio of 1:1 NaP:HAp nanocomposite has a higher efficiency in removal of fluoride ions than another ratios, Therefore, this adsorbent was considered as an effective adsorbent and was used for further study as well. Litrature reviews show that HAp is widely employed for the removal of fluoride from aqueous solution [40, 41]. Although HAp has excellent compatibility properties, its application is limited due to poor mechanical property of this material [42, 43]. Decomposition of the HAp into some calcium phases such as tricalcium phosphate (TCP) and tetra-calcium phosphate (TTCP) can be the main reason of loss in mechanical property of HAp [44]. It seems small amount of HAp that incorporated onto pores zeolite can be caused increasing stability of zeolite, however, with increasing amount of hydroxyapatite in NaP:HAp nanocomposite, some percent of HAp distributed over the external surface of zeolite. Furthermore, decreased efficiency of adsorbent may be occurred by transformation of HAp to phosphate phases.

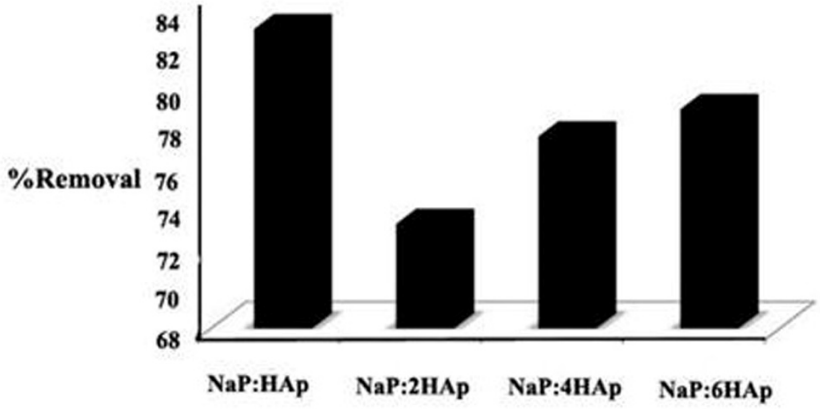


Fig.8. Percent removal of fluoride ion by different ratio of NaP:HAp

**3.3.2. Effect of pH value**

The correlation between pH factor with initial concentration, adsorbent dosage and temperature was shown by Fig 9, 10 and 11 respectively. It can be distinguished that the maximum removal of fluoride ion was found in the pH of 5-8 with removal percentage of 96.34% which is suitable for practical application in the household system and it seems, there are electrostatic attraction between the positively charged of metal in zeolite and hydroxyl apatite surface and fluoride anions [45]. Additionally, fluoride removal rate dramatically decreased below pH 5 and above pH 11. The decrease in the amount of removal fluoride in the alkaline range probably is due to competition of hydroxyl ions and fluoride ion on adsorption sites. On the other hand, under acidic condition range, the decrease may also be due to the formation of weakly ionized hydrofluoric acid [46]. Moreover, literature reviews show [47] that in the other nanocomposite, HAp may be partially dissolved at low pH, However, we investigated the FT-IR, XRD and $PO_4^{3-}$ and $Ca^{2+}$ concentration of adsorbent (1:1 ratio of NaP:HAp) after treatment with acid but there was not any drastic changes in the spectrum and they were like fresh adsorbent (Fig.12 ).

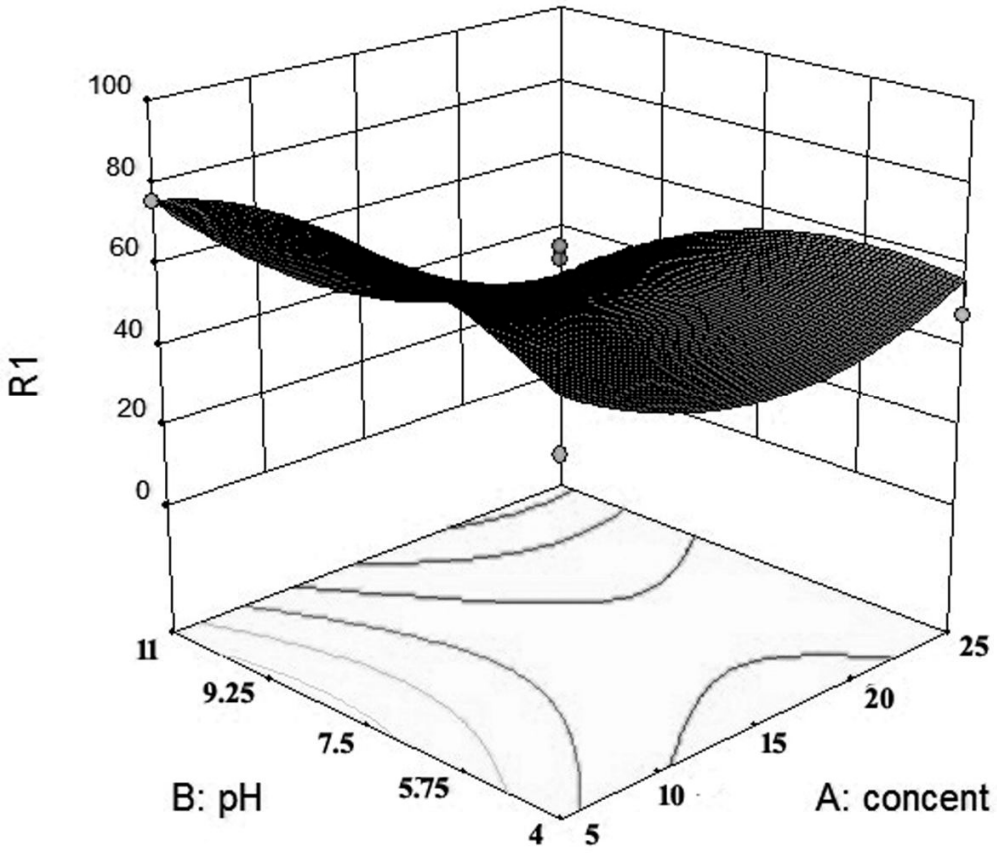


Fig.9. Response surface plot showing the effect of initial concentration and pH on $F^-$ removal at fixed adsorbent dose of NaP: HAp and T: 3 g/L and 55 ˚C, respectively.

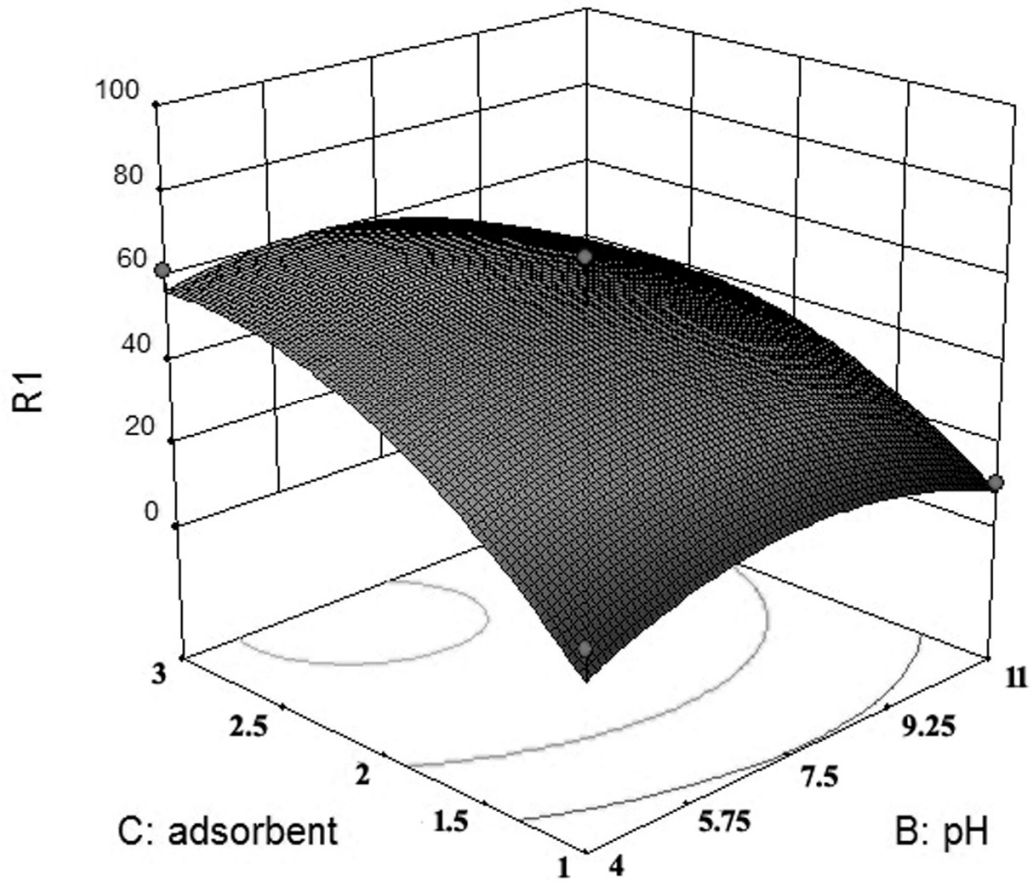


Fig.10. Response surface plot showing the effect of adsorbent dose and pH on $F^-$ removal at initial concentration and T: 5 mg/L and 55˚C, respectively.

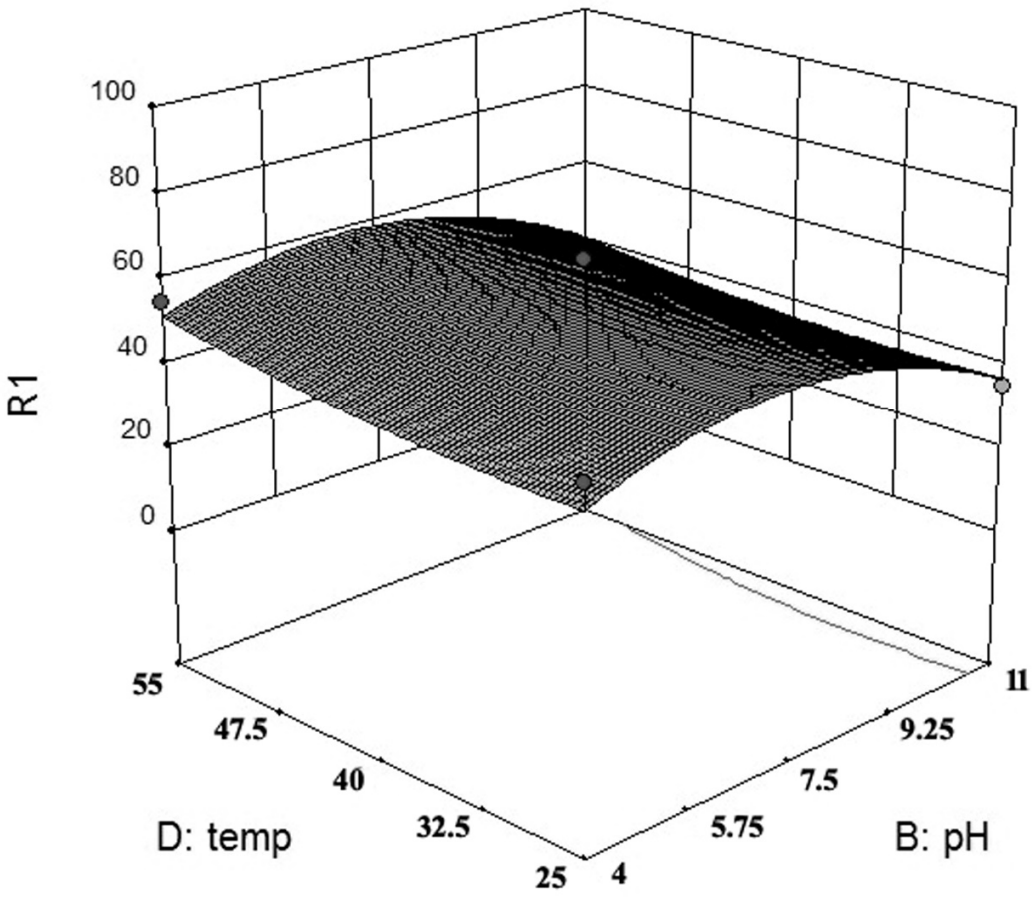


Fig.11. Response surface plot showing the effect of pH and temperature on $F^-$ removal at initial concentration and adsorbent dosage: 5 mg/L and 3 g/L, respectively.

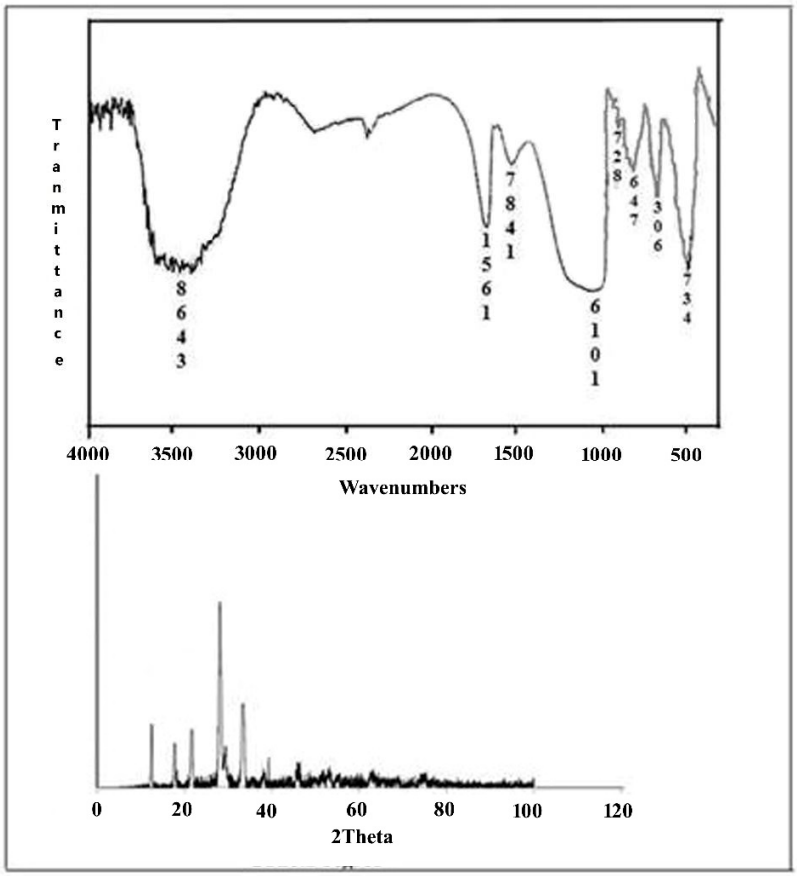


Fig.12. FT-IR and XRD of NaP: HAp nanocomposite with ratio of 1:1 after treatment with acid solution

**3.3.3. Effect of initial concentration**

To find initial concentration effect, the study was conducted with different concentration at 5, 10, 15, 20, 25 mg/L. The results of this effect are shown in Fig 9, 13 and 14. These figures clearly indicate that the highest removal efficiency was obtained at 5 mg/L initial concentration (97.1%). Also, it is clear from Fig 13 that increasing initial concentration has decreased removal efficiency effect. That event can be due to the fact that in high adsorbate concentration, the binding capacity adsorption gets exhausted slowly and resulting in a decrease in the total percent removal. This effect can be due to saturation of available surface area by fluoride ion as well [48]. Furthermore, the results confirm the increasing amount of the fluoride ions adsorbed per unit mass of the adsorbent with the increase of the initial concentration and this fact may be related to the high available number of fluoride ions per unit mass of adsorbent [49].

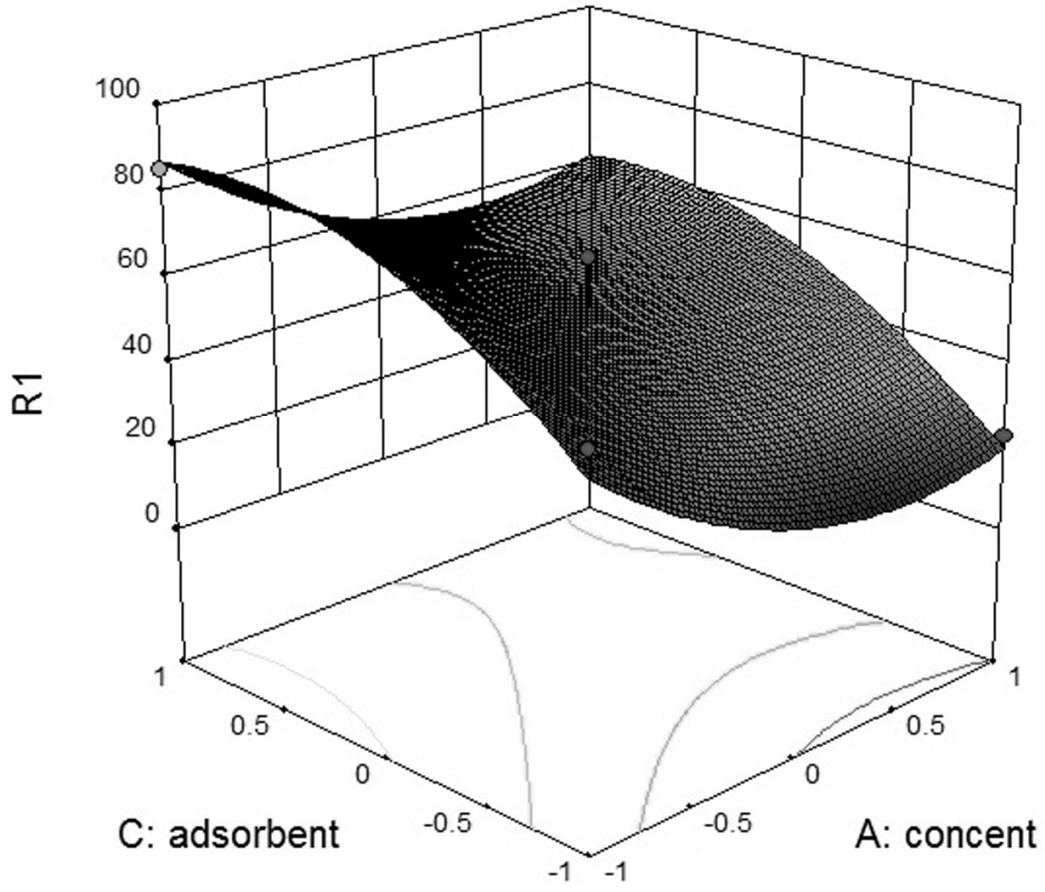


Fig.13. Response surface plot showing the effect of adsorbent dose and initial concentration on $F^-$ removal in pH and T: 7 and 55˚C, respectively.

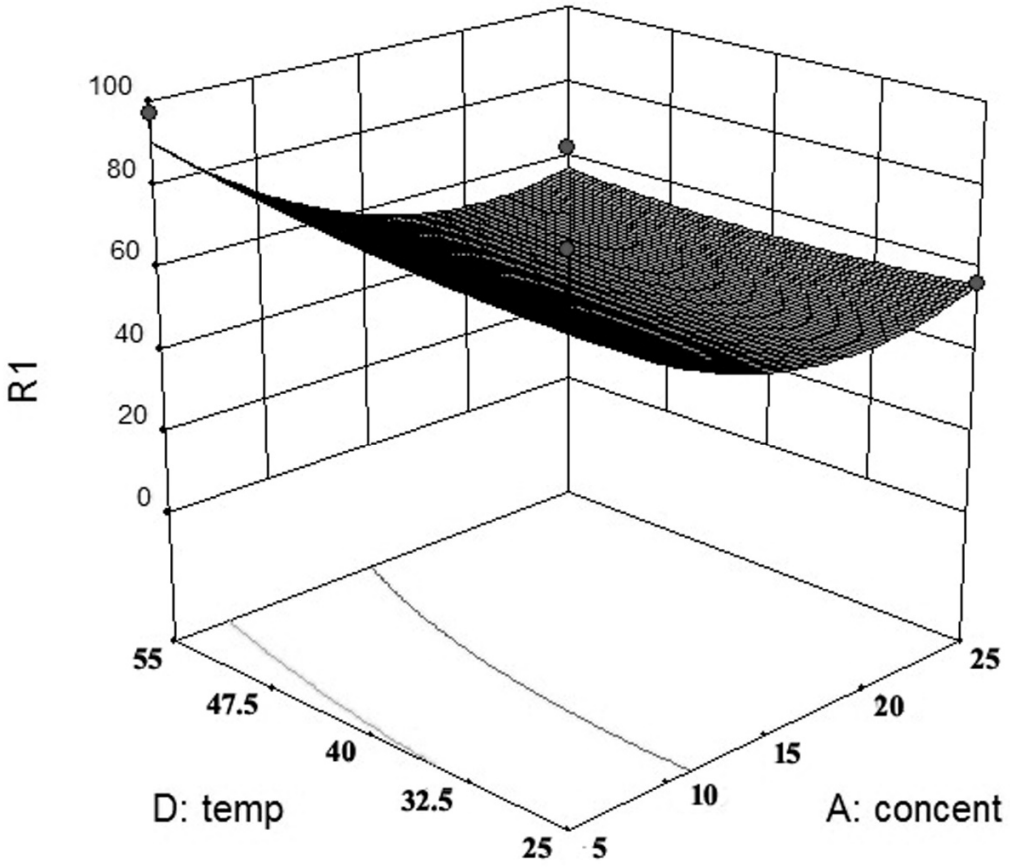


Fig.14. Response surface plot showing the effect of temperature and initial concentration on $F^-$ removal in pH and adsorbent dosage: 7 and 3 g/L, respectively.

**3.3.4. Effect of adsorbent dosage**

Adsorbent dosage is a significant factor because this determines the capacity of an adsorbent for given initial concentration of the fluoride ion at the operating conditions. In this part, combined effect of adsorbent dosage with initial concentration, pH and temperature were studied. It was observed that with increasing of adsorbent dosage, the amount of fluoride adsorbed increases, As it was cleared that whilst the amount of NaP: HAp nanocomposite was increased from 1 g/L to 3 g/L, removal efficiency of the fluoride ion increased from 75% to 90%. Thus, It can be concluded that the increase in fluoride removal efficiency was due to that the addition of availability of active sites for uptake of fluoride from solution (Fig.10, 13 and 15) [50].

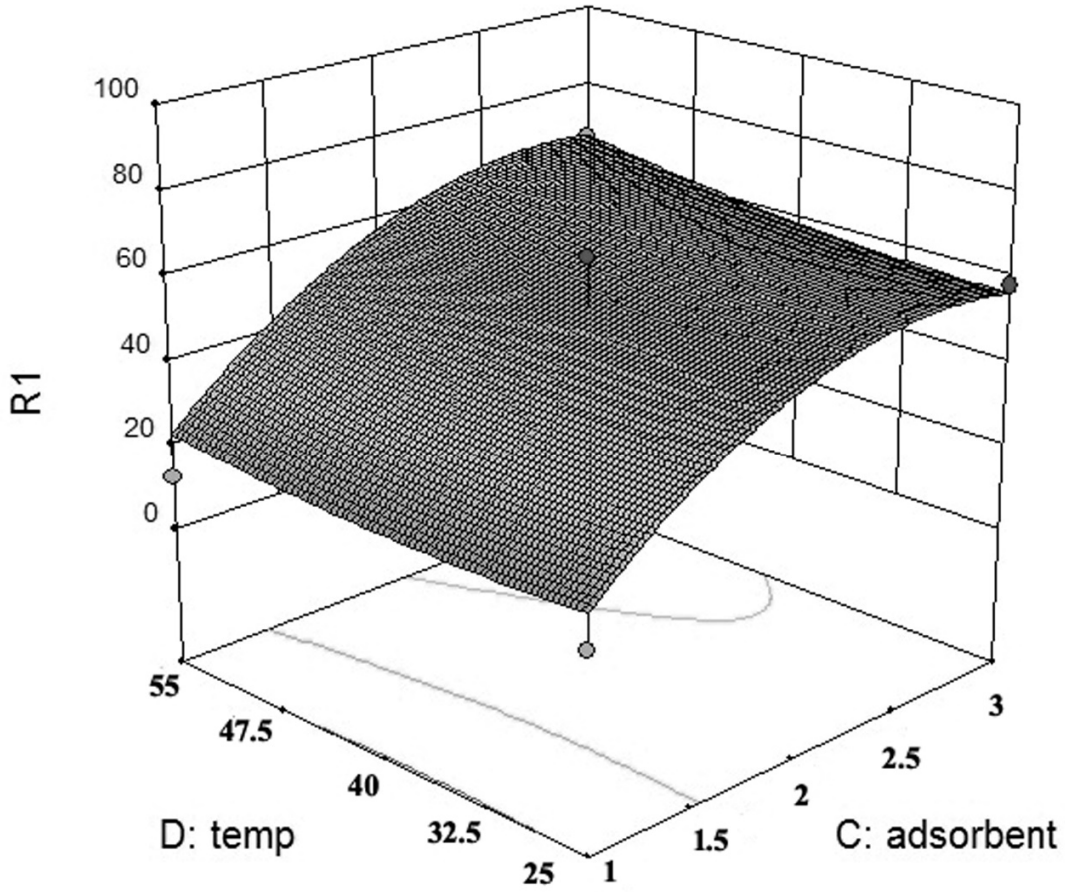


Fig.15. Response surface plot showing the effect of temperature and adsorbent dosage on $F^-$ removal in pH and initial concentration: 7 and 5 mg/L, respectively.

### 3.3.5. Effect of temperature and thermodynamic investigation

In order to study of the temperature effect on the removal efficiency, the adsorption experiments were conducted in temperature range 25˚- 55˚C. Fig.11. 14 and 15, show the effect of temperature on adsorption while keeping two parameters constant. It was found that the percentage of fluoride ions removed increases slowly with increasing in solution temperature from 25˚ to 55˚C, indicating that the adsorption is endothermic process. This was further supported by calculating of thermodynamic parameters such as Gibbs free energy (ΔG˚), entropy (ΔS˚) and enthalpy (ΔH˚). The changes in these parameters of adsorption can be determined by the following equations [51]:

$$\text{Log } K_c = \frac{\Delta S}{2.303R} - \frac{\Delta H}{2.303RT} \quad (5)$$

$$\Delta G = \Delta H - T\Delta S \quad (6)$$

Where, ΔH and ΔS are the changes in enthalpy and entropy of adsorption, respectively and R refers to the universal gas constant (8.314 Kj/mol.K). $K_c$ value is the equilibrium constant and calculated from Langmuir isotherm. Values of ΔH and ΔS were calculated from the slope and intercept of Vant Hoff plot (Log $K_c$ versus 1/T) and represented in Table 7. The Gibbs free energy change values in each temperature were found as negative which indicates the spontaneity and feasibility of the adsorption and the positive value of enthalpy indicates that the endothermic process of adsorption. The positive value of ΔS suggests that the entropy is responsible for making the ΔG negative value. Therefore, the adsorption process was spontaneous.

**Thermodynamic parameters**

| Temperature(˚C) | ΔG(KJ/mol) | ΔH(KJ/mol) | ΔS(J/mol.K) | $R^2$ |
|---|---|---|---|---|
| 25 | -3.181 | | | |
| 35 | -3.779 | | | |
| 45 | -4.177 | | | |
| 55 | -5.004 | 10.81 | 47.173 | 0.966 |

Table.7. Thermodynamic parameters of fluoride ion on NaP: HAp nanocomposite.

**3.3.6. Effect of contact time and adsorption kinetic**

Contact time as an important parameter in the adsorption dynamic was used in this study. The effect of contact time on adsorption of fluoride on NaP:Hydroxyapatite nanocomposite was shown in Figure 16. It was observed that fluoride uptake increases with time and gradually reaches equilibrium after 60 min. therefore 60 min was fixed as minimum contact time for efficient fluoride of sorbent.

The kinetic experiment was carried out for different contact time (5, 15, 30, 45, 60, 75, 90, 105, 120 min) with other optimum conditions such as 3 g/L of adsorbent, 5 mg/L initial concentration and pH of 7 at 55˚C. This kinetic experiment revealed that a contact time of 60 min was sufficient to reach equilibrium of fluoride onto NaP:HAp nanocomposite (Fig.17). Also, pseudo-second-order kinetic model is one of the commonly kinetic model was used in order to analyze the adsorption data. The pseudo-second-order kinetic model can be described by the following equation [52]:

$$(\frac{t}{q_t}) = \frac{1}{k_2 q_e^2} + \frac{1}{q_e}(t) \qquad (7)$$

Where $k_2$ is the rate constant of second-order rate adsorption in (g $mg^{-1}min^{-1}$), $q_t$ is the amount of fluoride adsorbed by adsorbent at any time (mg/g), $q_e$ is equilibrium adsorption and can be calculated from slope of the plot obtained by plotting $\frac{t}{q_t}$ versus t. Furthermore, $k_2$ can be determined from intercept of this plot. According to the high regression coefficient ($R^2$ = 0.9989), the kinetic of fluoride adsorption onto NaP:HAp nanocomposite fit well with the pseudo-second-order kinetic model.

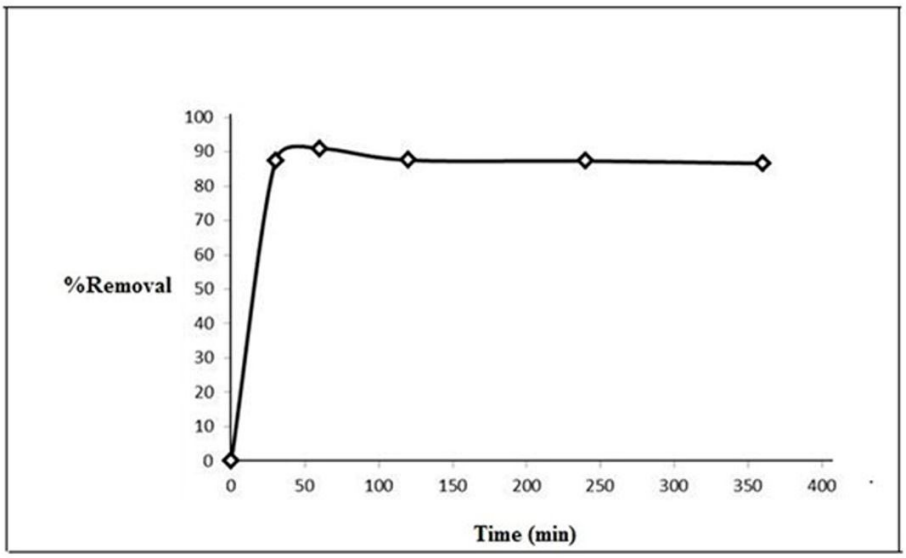


Fig.16. Effect of contact time of NaP:HAp nanocomposite on fluoride adsorption, adsorption condition: 3 g/L of adsorbent, 5mg/L of fluoride solution with pH 7.

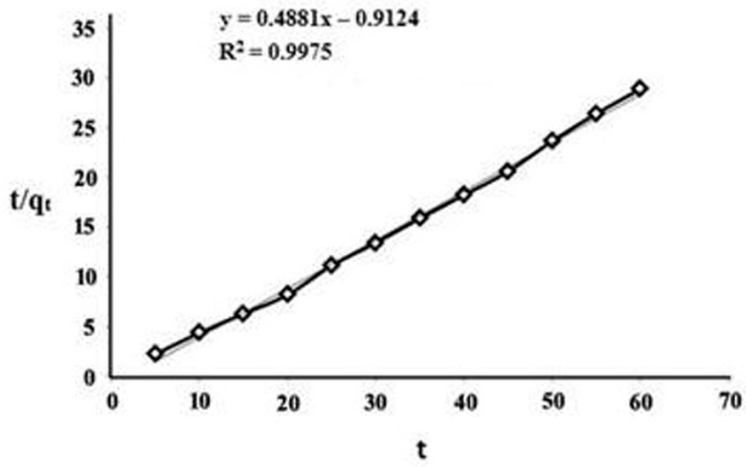


Fig.17. the pseudo-second order kinetic model of fluoride adsorption onto NaP:HAp nanocomposite.

**3.4. Optimization of adsorption process**

Optimization of the process, using the model at an initial F concentration of 5 mg/l, at pH of 7.5, a NaP:HAp nanocomposite dosage of 3g/L and 55˚C, resulted in 97.45% F removal that shown in Fig.18. These optimum conditions were evaluated experimentally and the result was close to the model (96.3%). The good correlation between theoretical and experimental results confirmed that Box-Behnken design could be effectively used to optimize the adsorption parameters for the removal of fluoride.

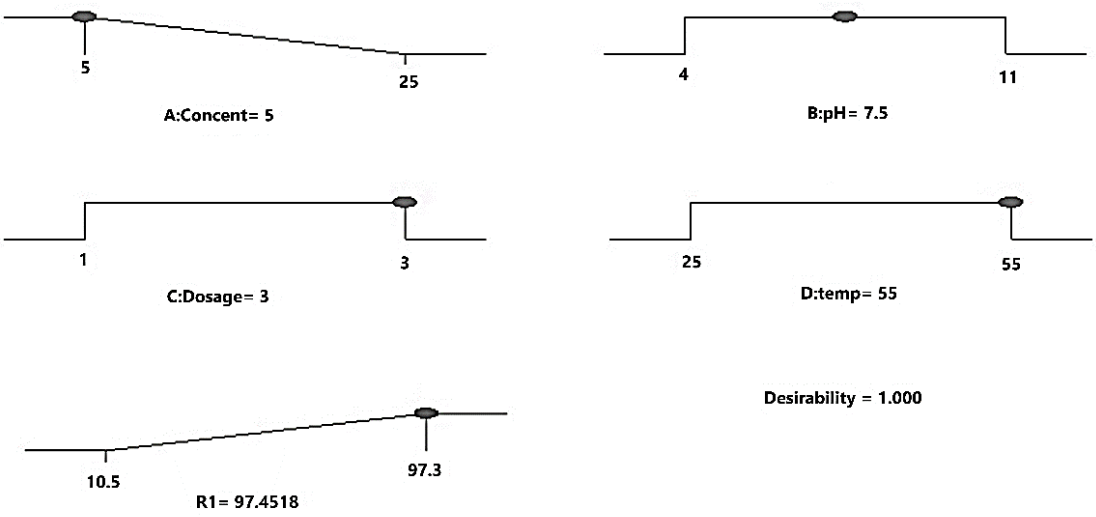


Fig.18. Desirability ramp for optimization of four parameters

### 3.5. Adsorption isotherms

In batch tests, Fig 19 reveals the plot of $\frac{Ce}{qe}$ versus Ce in temperature range of 25˚- 55˚C. This figure shows a straight line in all temperature which means that the equilibrium data were fitted to linearly transformed Langmuir isotherm. The linear form of Langmuir isotherm is expressed as [53]:

$$\frac{Ce}{qe} = \frac{1}{KL} + \frac{aL}{KL}(C_e) \qquad (8)$$

Where Ce is the equilibrium concentration (mg/L), qe is the amount of ion adsorbed (mg/g), $K_L$ is the equilibrium constant and the ratio of $a_L/K_L$ gives the inverse of theoretical monolayer saturation capacity ($q_m$). The result of fluoride ion sorption on NaP:HAp nanocomposite was also analyzed by use of Freundlich model to identified sorption behavior. The Freundlich equation has the general form [54]:

$$\text{Ln } q_e = \text{Ln } K_f + \frac{1}{n} \text{Ln } C_e \qquad (9)$$

Where qe is the amount of fluoride ion adsorbed per unit mass of adsorbent (mg/g), Ce is the equilibrium concentration of adsorbate (mg/L) and $K_f$ and n are Freundlich constant. From Fig 20, the plot of Ln qe versus Ln Ce, a straight line

with slope 1/n and intercept Ln $K_f$ is obtained. The Langmuir and Freundlich parameters for the adsorption of fluoride ion are given in Table 8.

In order to evaluate the nature of adsorption process as chemical or physical, the Dubinin–Radushkevich (D–R) isotherm model at optimum temperature (55˚C) was also used to analyze the equilibrium adsorption data. The linear form of D-R isotherm model was given by the following equation [55]:

$$Ln(q_e) = Ln(q_0) - K_D \varepsilon^2 \quad (10)$$

Where qe is the amount of adsorbate adsorbed per unit of adsorbent at equilibrium time (mg/g), $q_0$ is the maximum adsorption capacity (mg/g), $K_D$ is the isotherm constant related to the adsorption energy, ε is the Polanyi potential and equal to RT ln(1+1/Ce), R is the universal gas constant (8.314 J/molK), T is the temperature (kelvin), and Ce is the equilibrium concentration of adsorbate in solution (mg/L). The values of $q_0$ and $K_D$ can obtained from the slope and intercept of plot of Lnqe versus $\varepsilon^2$. The parameters of D-R isotherm model for adsorption of NaP:HAp nanocomposite were calculated and shown in Table 8. The value of mean free energy of adsorption (E) can be determined as follow [55]:

$$E = (2K_D)^{-0.5} \quad (11)$$

The magnitude of E is useful to estimate of the adsorption process. If E value is below 8 Kj/mol, the adsorption type is physical adsorption, if this value is between 8 kj/mol and 16 kj/mol, the adsorption type can be explained by ion exchange process and if the value of E is between 16 Kj/mol and 40 Kj/mol, the adsorption type is chemical process [55]. Therefore, according to data from Table 8, the value of E is below of 8 Kj/mol, Hence, the adsorption of fluoride onto NaP:HAp nanocomposite is a physical process.

| | **Langmuir constant** | | | **Freundlich constant** | | | **D-R constant** | | | |
|---|---|---|---|---|---|---|---|---|---|---|
| **Temperature(˚C)** | $q_m$ | $K_L$ | $R^2$ | $K_f$ | 1/n | $R^2$ | $K_D$ | $Lnq_0$ | E(Kj/mol) | $R^2$ |
| **25** | 11.947 | 3.612 | 0.9955 | 1.901 | 0.7472 | 0.9974 | - | - | - | - |
| **35** | 11.428 | 4.376 | 0.9952 | 2.553 | 0.7462 | 0.9826 | - | - | - | - |
| **45** | 12.269 | 4.859 | 0.9959 | 2.895 | 0.7388 | 0.9788 | - | - | - | - |
| **55** | 12.69 | 6.27 | 0.9933 | 3.607 | 0.7294 | 0.981 | $7\times10^{-8}$ | 2.0506 | 2.672 | 0.978 |

Table.8. Langmuir and Freundlich sorption isotherm constant and correlation coefficient ($R^2$) for fluoride ion on NaP:HAp nanocomposite.

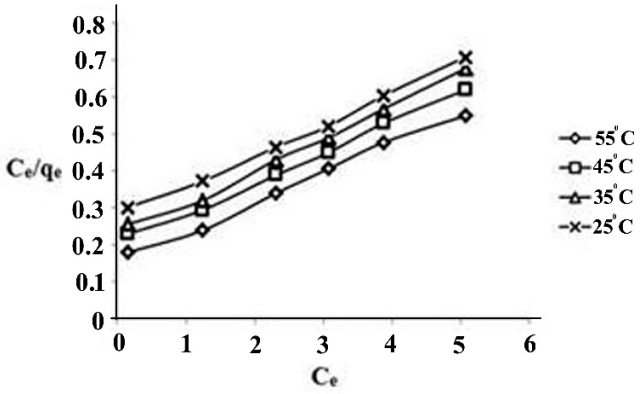


Fig.19. Langmuir isotherm model in different temperature

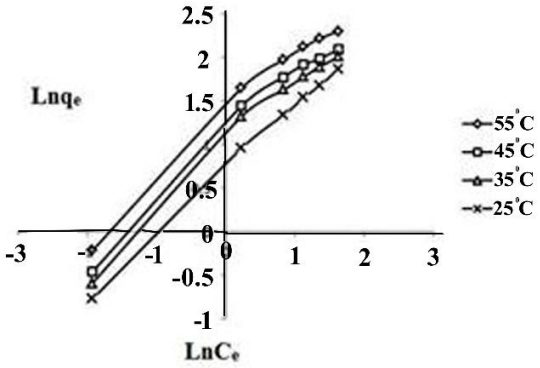


Fig.20. Freundlich isotherm model in different temperature

**3.6. Desorption study**

Desorption study gives knowledge about nature of adsorption. In order to study of the desorption, after first adsorption of fluoride ions by NaP:HAp nanocomposite, the waste of adsorbent putted in the 25 mL of 0.1 N hydrochloric acid solution for 1h and then, the filtrate was measured for fluoride content. After that, this adsorbent was floated in the desired solution (pH of 7 at 55˚C and 3 g/L of adsorbent with 5 mg/L of fluoride solution) for 1h and concentration of residue ions was determined as well and this cycle was repeated for 10 times. Also, the same condition was carried out for sodium hydroxide solution (0.1 N of NaOH) to recognize the reuse-ability of NaP:HAp nanocomposite in

acidic and alkaline solution. These results were compared and demonstrated in Fig 21. As shown in Fig 21, desorption of adsorbed fluoride in acidic solution and alkaline solution resulted about 65.2% and 51% respectively. It is evident from high desorption values in both solutions that the adsorption of fluoride on to NaP:HAp nanocomposite was physical in nature. This result is according to E value calculated by D-R isotherm in 3.5. Section.

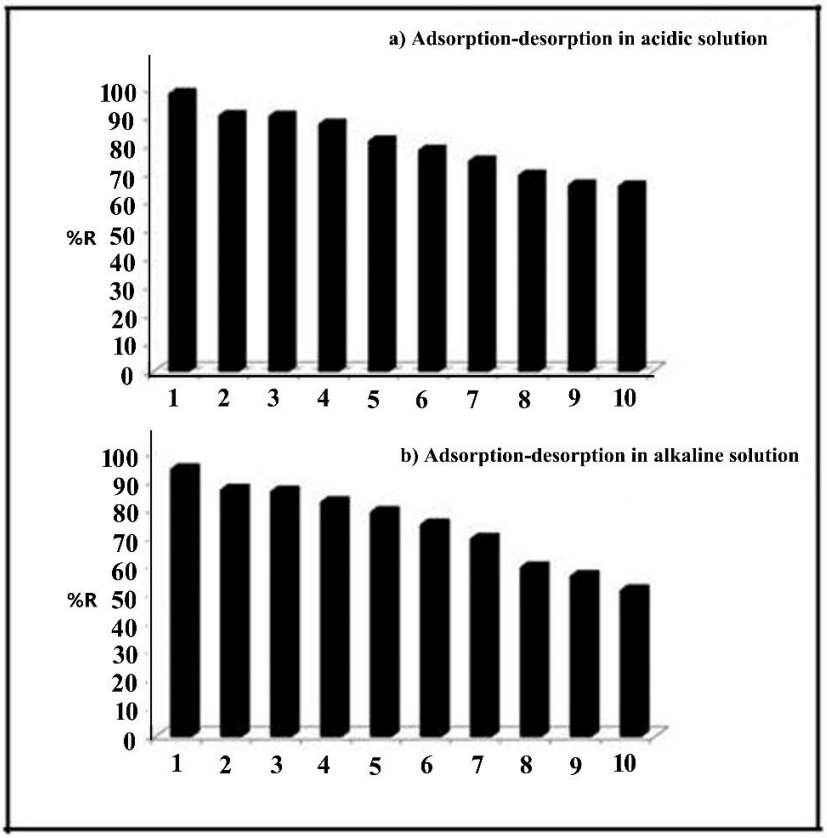


Fig.21. a) Adsorption-desorption in acidic solution, b) Adsorption-desorption in alkaline solution

### 3.7. Mechanism of fluoride sorption on NaP:HAp nanocomposite

The fluoride removal by NaP:HAp can be controlled by both adsorption and ion exchange mechanisms. Theoretically, three essential steps can be taken during removal process of fluoride onto solid particles [56]:

a) External mass transfer has been occurred by transfer or diffusion of fluoride ions to the external surface adsorbent from bulk solution;

b) Particle surfaces adsorbed fluoride ions;

c) It is possible that the adsorbed fluoride ions exchange with the structural elements inside adsorbent particle;

Whereas, NaP:HAp nanocomposite contains two parts of zeolite and hydroxyapatite so the mechanism of fluoride removal can be described by both reactions in zeolite and hydroxyapatite.

As described above, some percent of HAp is distributed onto external surface of zeolite, so fluoride ions get adsorbed onto hydroxyapatite and the OH group presents in the hydroxyapatite can be exchanged with fluoride ions and caused formation of fluorapatite or hydroxyfluorapatite that indicates according the reaction [57]:

$$Ca_{10}(PO_4)_6(OH)_2 + 2F^- \longrightarrow Ca_{10}(PO_4)_6(F)_2 + 2OH^- \quad (12)$$

or

$$Ca_{10}(PO_4)_6(OH)_2 + F \longrightarrow Ca_{10}(PO_4)_6\,FOH + OH^- \quad (13)$$

In addition, zeolite part in nanocomposite has an efficient role in removal of fluoride. Hydrolysis process of zeolite illustrated according the reaction [58]:

$$Me\text{-}Z\ (s) + H_2O\ (l) \longleftrightarrow H\text{-}Z + Me^{n+} + nOH^- \quad (14)$$

Where Z is zeolite, Me is an exchangeable cation ($Na^+$, $K^+$, $Ca^{2+}$, $Mg^{2+}$) and n is cation charge. A reaction of metallic ions occurs at the same time:

$$Me^{n+}\ (l) + H_2O\ (l) \longleftrightarrow [Me\text{-}OH]^+ + H^+ \quad (15)$$

According to the latest reaction, adsorbed fluoride ions onto zeolite surface can be exchanged with OH group that adsorbed onto the surface zeolite and it is possible that fluoride anions on the zeolite surface form with exchangeable cations more or less stable complexes:

$$Me^{n+}\ (l) + mA^{y-}\ (l) \longleftrightarrow (MeA_m)^{n-my}\ (l) \quad (16)$$

Hence, it can be concluded that the fluoride removal by NaP:HAp nanocomposite is carried out by both adsorption and ion exchange mechanisms and thus it can act as an effective adsorbent.

**3.8. Removal of fluoride from real water sample**

In order to investigate efficiency of NaP:HAp nanocomposite on removal of fluoride ion in real case, this adsorbent was tested for detection of $F^-$ in sea water of Persian Gulf (latitude 27˚49′94″, longitude 52˚62′19″). The values of fluoride anion in sea water as an unknown sample from the standard plot was measured 1.241 ppm and the result presented in Fig 22 (a). Four different ratio of nanocomposite (NaP:HAp ratio: 1:1, 1:2, 1:4 and 1:6) was tested and results were showed in Fig 22 (b). It is evident from these results that NaP:HAp with ratio of 1:1 showed the best

efficiency in removal of fluoride anion from sea water. This result is in good according with above data about high effect of NaP:HAp nanocomposite in removal of fluoride from aqueous solution in section 3.3.1.

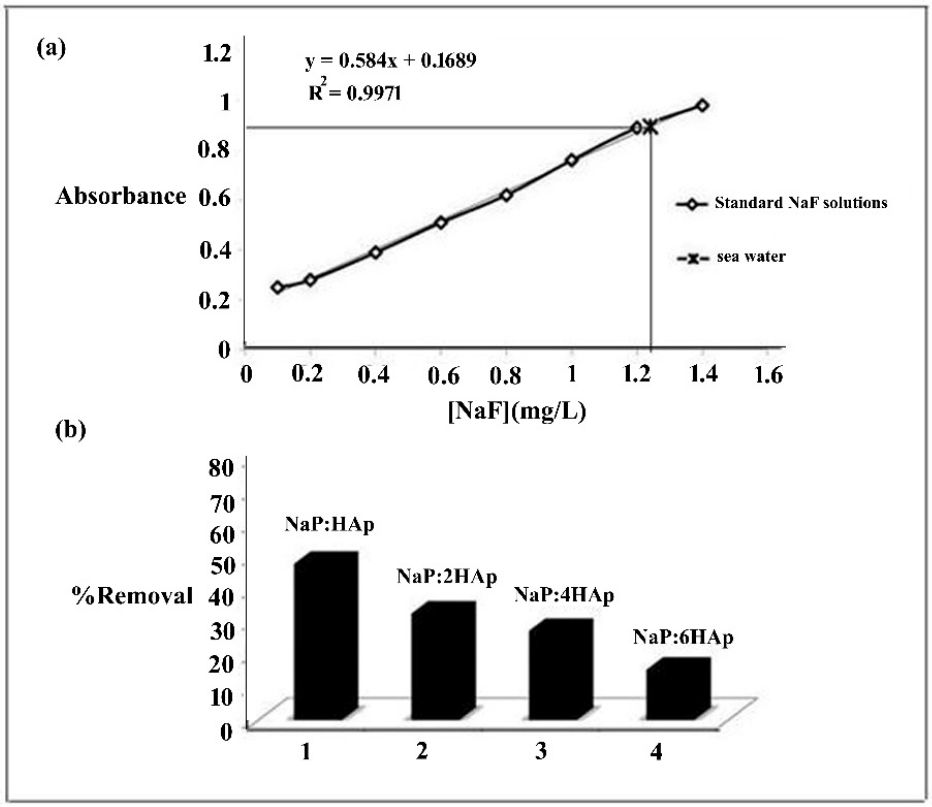


Fig.22. (a) Calibration curve for determination of fluoride ion from sea water, (b) Removal percent of fluoride ion sea water by different ratio of NaP:HAp nanocomposite

**3.9. Comparison of fluoride removal with other adsorbent**

Table 9 shows the comparison between NaP:HAp nanocomposite and previously reported adsorbents for uptake of fluoride from aqueous solution. The maximum capacity of fluoride adsorption of NaP:HAp nanocomposite is higher than many other adsorbents. The high fluoride adsorption capacity obtained in this study is mainly due to the dispersion of metals in the NaP:HAp nanocomposite adsorbent. These elements have a strong affinity with fluoride ions. Therefore, synthesized nanocomposite adsorbent that is easy to implement is effective adsorbent for removing fluoride from aqueous solution as well.

| adsorbent | $q_m$ | refrences |
|---|---|---|
| Hydroxyapatite | 3.12 | [39] |
| granular ceramic | 0.941 | [2] |
| charred beef shoulder blade bones | 3.154 | [59] |
| natural stilbite zeolite modified with Fe(III) | 2.31 | [60] |
| ceramic adsorbent | 2.16 | [5] |
| AlFe650/C | 13.64 | [15] |
| Carbon slurry | 4.86 | [61] |
| Activated alumina | 2.41 | [62] |
| NaP:HAp nanocomposite | 12.69 | Present study at optimum temperature |

Table.9. Comparison between various adsorbents used for uptake of fluoride.

**4. Conclusion**

In this paper, NaP:HAp nanocomposite as an efficient adsorbent was synthesized by hydrothermal process. The product was ascertained by various characterizing such as: FT-IR, XRD, SEM, EDAX, BET and TG/DTA. The response surface methodology was combined by Box-Behnken design to determine the effect of four process factors such as initial concentration, initial pH, adsorbent dosage and temperature on fluoride removal. The results showed that the second-order polynomial regression model was capable accurately interpreting the experimental data with the coefficient of determination ($R^2$) value of 0.9327 and an F-value of 13.87. Optimum pH value was found to be 7 at 60 min with 5 mg/L of fluoride concentration. It is evident from the dosage study that there was increase in percentage removal for increase in dosage from 1 g/L to 3 g/L. in temperature study, it was found that the removal capacity increases by increasing temperature from 25 ˚C to 55˚C, indicating that the adsorption is endothermic process. Adsorption of fluoride was found to follow second order kinetics. The adsorption isotherm was evaluated by various models such as Freundlich, Langmuir and Dubinin–Radushkevich isotherm model and it was correlated well with the Langmuir adsorption model. In addition, thermodynamic parameters such as Gibbs free energy (ΔG˚), entropy (ΔS˚) and enthalpy (ΔH˚) was investigated and the enthalpy data was revealed the endothermic in nature. Maximum capacity of adsorption was found to be 66.66 mg/g, and it indicated NaP:HAp nanocomposite can be used as an efficient adsorbent rather than many other adsorbents in terms of defluoridation capacity.

**Acknowledgment**: Thanks are due to the Iranian Nanotechnology Initiative and the Research Council of Arak University of Technology and Center of Excellence in the Chemistry Department of Arak University of Technology for supporting of this work.

**References:**

[1] M. Koteswaro Rao, M. Mallikarjum, Effective low cost adsorbents for removal of fluoride from Water: A Review, International, journal of science and research. 3 (2014) 2319-7064.

[2] N. Chen, Z. Zhang, Ch. Feng, N. Sugiura, M. Li, R. Chen, Fluoride removal from water by granular ceramic adsorption, J. Colloid and Interface Science. 348 (2010) 579–584.

[3] X. Zhao, J. Wang, F. Wu, Th. Wang, Y. Cai, Y. Shi, G. Jiang, Removal of fluoride from aqueous media by $Fe_3O_4$@$Al(OH)_3$ magnetic nanoparticles, J. Hazardous Materials. 173 (2010) 102–109.

[4] A. Jafari, A.H. Mahvi, H. Godini, R. Rezaee, S.S. Hosseini, Process optimization for fluoride removal from water by moringa oleifera seed extract. research report fluoride. 47 (2014) 152-160.

[5] N. Chen, Z. Zhang, Ch. Feng, M. Li, D. Zhu, R. Chen, N. Sugiura, An excellent fluoride sorption behavior of ceramic adsorbent, J. Hazardous Materials. 183 (2010) 460–465.

[6] S. Meenakshi, N. Viswanathan, Identification of selective ion-exchange resin for fluoride sorption, J. Colloid Interface Sci. 308 (2007) 438–450.

[7] S. Ghorai, K.K. Pant, Investigations on the column performance of fluoride adsorption by activated alumina in a fixed-bed, Chem. Eng. J. 98 (2004) 165–173.

[8] Y.H. Li, S. Wang, X. Zhang, J. Wei, C. Xu, Z. Luan, D. Wu, sorption of divalent metal ions from aqueous solution by oxidized carbon nanotubes and nanocages: Review, Mater. Res. Bull. 38 (2003) , 469–476.

[9] N.A. Medellin-Castillo, R. Leyva-Ramos, R. Ocampo-Perez, R.F.G. de la Cruz, A. Aragon-Pina, J.M. Martinez-Rosales, R.M. Guerrero-Coronado, L. Fuentes-Rubio, Adsorption of Fluoride from Water Solution on Bone Char, Ind. Eng. Chem. Res. 46 (2007) 9205–9212.

[10] E. Oguz, Equilibrium isotherms and kinetics studies for the sorption of fluoride on light weight concrete materials, Colloids and Surf. A: Physic ochem. Eng. Aspe. 295 (2007) 258–263.

[11] P. Miretzky, A.F. Cirelli, Fluoride removal from water by chitosan derivatives and composites: A review, J. Fluorine chemistry. 132 (2011) , 231–240.

[12] X.L. Zhao, Y.L. Shi, Y.Q. Cai, S.F. Mou, Cetyltrimethylammonium Bromide-Coated Magnetic Nanoparticles for the Preconcentration of Phenolic Compounds from Environmental Water Samples, Environ. Sci. Technol. 1139 (2008) 178–184.

[13] D. Zhang, H. luo, L. Zheng, K. Wang, H. Li, Y. Wang, H. Feng, Utilization of waste phosphogypsum to prepare hydroxyapatite nanoparticles and its application towards removal of fluoride from aqueous solution, J. Hazardous materials. 241-242 (2012) 418-426.

[14] A. Banerjee, A. Bandyopadhyay, S. Bose, Hydroxyapatite nanopowders: Synthesis, densification and cell–materials interaction, J. Materials Science and Engineering C. 27 (2007) 729–735.

[15] Y. Sun, Q. Fang, J. Dong, X. Cheng, J. Xu, In Situ Crystallization of Macroporous Monoliths with Hollow NaP Zeolite Structure,Desalination. 277 (2011) 121–127.

[16] Y. Huang, D. Dong, J. Yao, L. He, J. Ho, Ch.Ch. Kong, A.J. Hill, H. Wang, In Situ Crystallization of Macroporous Monoliths with Hollow NaP Zeolite Structure, J. Chem matter. 22 (2010) 5271-5278.

[17] U. Kakansson, L. Falth, S. Hansen, Structure of a high-silica variety of zeolite Na-P, Acta.Cryst. C46 (1990) 1363-1364.

[18] D.C. Montgomery, Design and Analysis of Experiments, 5th Edn., John Wiley and Sons, New York, 2001.

[19] R.H. Myers, D.C. Montgomery, C.M. Anderon-Cook, Response Surface Methodology: Process and Product Optimization Using Designed Experiments, Wiley, New York, 2009.

[20] H. Khanmohammadi, Kh. Rezaeian, Naked-eye detection of inorganic fluoride in aqueous media using a new azo-azomethine colorimetric receptor enhanced by electron withdrawing groups, Rsc Advances. 4 (2014) 1032-1038.

[21] M. Evans, Optimization of Manufacturing Processes: A Response Surface Approach, Maney Publishing, London, 2003.

[22] P.R. Choudhury, P. Mondal, S. Majumdar, Synthesis of bentonite clay based hydroxyapatite nanocomposites cross-linked by glutaraldehyde and optimization by response surface methodology for lead removal from aqueous solution, RSC Advances. 5(122) (2015) 100838-100848.

[23] K. Benyounis, A. Olabi, M. Hashmi, Effect of Laser Welding Parameters on the Heat Input and Weld-bead Profile, J. Mater. Process. Technol. 164-165 (2005) 978-985.

[24] A.N. Ejhieha, M. Khorsandi, Photodecolorization of Eriochrome Black T using NiS–P zeolite as a heterogeneous catalyst, J. Hazardous Materials. 176 (2010) 629-637.

[25] A.H. Alwash, A.Z. Abdullah, N. Ismail, Zeolite Y encapsulated with Fe-$TiO_2$ for ultrasound-assisted degradation of amaranth dye in water, J. Hazardous Mater. 233-234 (2012) 184-193.

[26] M. Abecassis.Wolfovich, R. Jothiramalingam, M.V. Landau, M. Herskowitz, B. Viswanathan, T.K. Varadarajan, Cerium incorporated ordered manganese oxide OMS-2 materials: Improved catalysts for wet oxidation of phenol compounds, Appl. Catal. B: Environ. 59 (2005) 91-98.

[27] S. Hansen, U. Hakansson, L. Faelth, structure of synthetic zeolite Na-P2, Section C: Crystal Structure Communications. 46 (1990) 1361-1362.

[28] H.El. Feki, J.M. Savariault, Ben. Salah, Structure refinements by the Rietveld method of partially substituted Hydroxyapatite $Ca_9Na_{0.5}(PO_4)_{4.5}(CO_3)_{1.5}(OH)_2$, J. Alloys and Compounds. 287 (1999) ,114-120.

[29] M. Sadeghi, S.L. Sharifi, H. Hatami, Synthesis of nanocrystalline zeolite NaY by Hydrothermal method and investigation of its structure and morphology, Int. J.Nano Dimens. 5 (2014) 91-95.

[30] Y. Zhan, J. Lin, J. Li, Preparation and characterization of surfactant-modified hydroxyapatite/zeolite composite and its adsorption behavior toward humic acid and copper(II), Environ SciPollut Res. 20 (2013) 2512-2526.

[31] Y. Wang, S. Zhang, KWei, NZhao, JChen, X. Wang, Hydrothermal synthesis of hydroxyapatite nanopowders using cationic surfactant as a template. Materials Letters. 60 (2006) 1484–1487.

[32] Z. Huo, XXu, Z. Lü, J. Song, M. He, Z. Li, Q. Wang, L. Yan, Synthesis of zeolite NaP with controllable morphologies, Microporous and Mesoporous Materials. 158 (2012) 137–140.

[33] K.J. Balkus, A.G. Gabrielov, Zeolite Encapsulated Metal Complexes, J. Inclu. Phenom. Mol. Recognition Chem, 21 (1995) 159-184.

[34] A. Corma, From Microporous Molecular sieve Materials and Their Use in Catalysis, Chem. Rev. 97 (1997) 2373–2419.

[35] G. Cruciani, Zeolites upon heating: Factors governing their thermal stability and structural changes, Journal of Physics and Chemistry of Solids. 67 (2006) 1973-1994.

[36] D.W. Breck, Zeolite Molecular Sieves: Structure, Chemistry and Use, John Wiley & Sons, New York, 1974.

[37] S. Singh, S.B. Jonnalagadda, synthesis of thermally stable metal substituted hydroxyl apatites for the selective oxidation of light paraffins, Bull. Chem. Soc. Ethiop, 27 (2013) 57-68.

[38] M. Zendehdel, H. Khanmohamadi, M. Mokhtari, Host (nano cage NaY)/guest Mn(II), Co(II), Ni(II) and Cu(II) Complexes of N,N-bis(3,5-di-tert-butylsalicyidene)-2,2-dimethyle-1,3-diaminopropane: Synthesis and Catalyst Activity, J. Chin. Chem. Soc. 57 (2010) 205-212.

[39] M. Mourabet, A. El Rhilassi, H. El Boujaady, M. Bennani-Ziatni, R. El Hamri, A. Taitai-Removal of fluoride from aqueous solution by adsorption on hydroxyapatite (HAp) using response surface methodology, Journal of Saudi Chemical Society. 19 (2015) 603-615.

[40] C.S. Sundaram, N. Viswanathan, S. Meenakshi, Defluoridation chemistry of synthetic hydroxyapatite at nano scale: equilibrium and kinetic studies, Journal of Hazardous Materials. 155(1) (2008) 206-215.

[41] S. Gao, R. Sun, Z. Wei, H. Zhao, H. Li, F. Hu, Size-dependent defluoridation properties of synthetic hydroxyapatite, Journal of Fluorine Chemistry. 130(6) (2009) 550-556.

[42] O. Prokopiev, I. Sevostianov, Dependence of the mechanical properties of sintered hydroxyapatite on the sintering temperature, Materials Science and Engineering: A. 431(1) (2006) 218-227.

[43] L.-H. He, O.C. Standard, T.T. Huang, B.A. Latella, M.V. Swain, Mechanical behaviour of porous hydroxyapatite, Acta Biomaterialia. 4(3) (2008) 577-586.

[44] I. Mobasherpour, M.S. Hashjin, S.R. Toosi, R.D. Kamachali, Effect of the addition $ZrO_2$–$Al_2O_3$ on nanocrystalline hydroxyapatite bending strength and fracture toughness, Ceramics International. 35(4) (2009) 1569-1574.

[45] A. Tor, N. Danaoglu, G. Arslan, Y. Cengeloglu, Removal of fluoride from water by using granular red mud: Batch and column studies, J. Hazard. Mater. 164 (2009) 271–278.

[46] Z. Jin, Y. Jia, T. Luo, L.T. Kong, B. Sun, W. Shen, F.L. Meng, J.H. Liu, Efficient removal of fluoride by hierarchical MgO microspheres: Performance and mechanism study, Applied Surface Science. 357 (2015) 1080-1088.

[47] Yu. Xiaolin, T. Shengrui, G. Maofa, Z. Junchao, Removal of fluoride from drinking water by cellulose@hydroxyapatite nanocomposites, Carbohydrate Polymers. 92 (2013) 269– 275.

[48] S.K. Swain, T. Patnaik, V.K. Singh, U. Jha, R.K. Patel, R.K. Dey, Kinetics, equilibrium and thermodynamic aspects of removal of fluoride from drinking water using meso-structured zirconium phosphate, Chemical Engineering Journal. 171 (2011) 1218– 1226.

[49] M. Karthikeyan, K.K. Satheesh Kumar, K.P. Elango, Conducting polymer/alumina composites as viable adsorbents for the removal of fluoride ions from aqueous solution, Journal of Fluorine Chemistry. 130 (2009) 894–901.

[50] A.E. YILMAZ, B.A. FIL, S. BAYAR, K. KARCIOĞLU, a new adsorption for fluoride removal: the utilization of sludge waste from electrocoagulation as adsorbent, Global NEST journal. 17 (2015) 186-197.

[51] M. Islam, R.K. Patel, Evaluation of removal efficiency of fluoride from aqueous solution using quick lime, J. Hazardous materials. 143(2007) 303–310.

[52] Y.S. Ho, G. McKay, Pseudo-second order model for sorption processes Process, Biochemistry. 34 (1999) 451–465.

[53] T.K. Saha, N.Ch. Bhoumik, S. Karmaker, M.Gh. Ahmed, H. Ichikawa, Y. Fukumori, Adsorption of Methyl Orange onto Chitosan from Aqueous Solution, J. Water Resource and Protection. 2 (2010) ,898-906.

[54] Ö. Yavuz, R. Guzel, F. Aydin, I. Tegin, R. Ziyadanogullari, Removal of Cadmium and Lead from Aqueous Solution by Calcite, Polish J. of Environ. Stud. 16 (2007) 467-471.

[55] H. Chen, J. Zhao, J. Wu, G. Dai, Isotherm, thermodynamic, kinetics and adsorption mechanism studies of methyl orange by surfactant modified silkworm exuviae, J. Hazardous Materials. 192 (2011) 246– 254.

[56] X. Fan, D. Parker, M. Smith, Adsorption kinetics of fluoride on low cost materials, Water Research. 37(20) (2003) 4929-4937.

[57] H.G. McCann, Reactions of fluoride ion with hydroxyapatite, Journal of Biological Chemistry. 201(1) (1953) 247-259.

[58] K. Margeta, A. Farkas, M. Šiljeg, N.Z. Logar, Natural zeolites in water treatment-how effective is their use. INTECH Open Access Publisher (2013).

[59] M. Gourouza, I. Natatou, A. Boos, Elimination of fluoride ions from an aqueous solution with charred beef shoulder blade bones, J. Mater. Environ. Sci. 5 (2014) 416-425.

[60] E. Tchomgui-Kamga, V. Alonzo, Ch.P. Nanseu-Njiki, N. Audebrand, E. Ngameni, A. Darchen, Preparation and characterization of charcoals that contain dispersed aluminum oxide as adsorbents for removal of fluoride from drinking water, CARBON. 48 (2010) 333 –343.

[61] V. Kumar Gupta, I. Ali, V. Kumar Saini, Defluoridation of wastewaters using waste carbon slurry, water research. 41 (2007) 3307–3316.

[62] S. Ghorai, K.K. Pant, Equilibrium, kinetics and breakthrough studies for adsorption of fluoride on activated alumina, Separation and Purification Technology. 42 (2005) 265–271.